cy 2

DETERMINATION OF THE SIZE DISTRIBUTION FUNCTION
FOR PARTICLES IN A HYPERSONIC FLOW FIELD

J. W. L. Lewis, B. P. Curry, and D. P. Weaver
ARO, Inc., a Sverdrup Corporation Company

VON KÁRMÁN GAS DYNAMICS FACILITY
ARNOLD ENGINEERING DEVELOPMENT CENTER
AIR FORCE SYSTEMS COMMAND
ARNOLD AIR FORCE STATION, TENNESSEE 37389

July 1978

Final Report for Period February - September 1977

Prepared for

ARNOLD ENGINEERING DEVELOPMENT CENTER/DOTR
ARNOLD AIR FORCE STATION, TENNESSEE 37389

This report has been reviewed by the Information Office (OI) and is releasable to the National Technical Information Service (NTIS). At NTIS, it will be available to the general public, including foreign nations.

APPROVAL STATEMENT

This report has been reviewed and approved.

STANISLAUS L. LUDWIG, Captain (CF)
Project Manager, Research Division
Directorate of Test Engineering

Approved for publication:

FOR THE COMMANDER

ROBERT W. CROSSLEY, Lt Colonel, USAF
Acting Director of Test Operations
Deputy for Operations

REPORT DOCUMENTATION PAGE		READ INSTRUCTIONS BEFORE COMPLETING FORM
1 REPORT NUMBER AEDC-TR-77-101	2 GOVT ACCESSION NO.	3 RECIPIENT'S CATALOG NUMBER
4 TITLE (and Subtitle) DETERMINATION OF THE SIZE DISTRIBUTION FUNCTION FOR PARTICLES IN A HYPERSONIC FLOW FIELD		5 TYPE OF REPORT & PERIOD COVERED Final Report - February - September 1977
		6 PERFORMING ORG. REPORT NUMBER
7 AUTHOR(s) J. W. L. Lewis, B. P. Curry, and D. P. Weaver, ARO, Inc.		8 CONTRACT OR GRANT NUMBER(s)
9 PERFORMING ORGANIZATION NAME AND ADDRESS Arnold Engineering Development Center/DOT Air Force Systems Command Arnold Air Force Station, Tennessee 37389		10. PROGRAM ELEMENT. PROJECT. TASK AREA & WORK UNIT NUMBERS Program Element 65807F
11 CONTROLLING OFFICE NAME AND ADDRESS Arnold Engineering Development Center/DOS Arnold Air Force Station, Tennessee 37389		12. REPORT DATE July 1978
		13 NUMBER OF PAGES 47
14 MONITORING AGENCY NAME & ADDRESS(if different from Controlling Office)		15. SECURITY CLASS. (of this report) UNCLASSIFIED
		15a DECLASSIFICATION/DOWNGRADING SCHEDULE N/A

16 DISTRIBUTION STATEMENT (of this Report)

Approved for public release; distribution unlimited.

17 DISTRIBUTION STATEMENT (of the abstract entered in Block 20, if different from Report)

18 SUPPLEMENTARY NOTES

Available in DDC

19 KEY WORDS (Continue on reverse side if necessary and identify by block number)

determination	particles
sizes	hypersonic
distribution	flow fields
functions	

20. ABSTRACT (Continue on reverse side if necessary and identify by block number)

The mean particle diameter and size distribution function of submicron particulate matter were determined for an arc-heated, short-duration flow field. From these measurements the particle number density and mass fraction in the flow were also estimated. The experiment provided approximately 10-msec time resolution and yielded the desired information by making use of both angular scattered intensity and degree of polarization measurements. The

DD FORM 1473 EDITION OF 1 NOV 65 IS OBSOLETE
1 JAN 73

20. ABSTRACT (Continued)

novel aspects of both the experimental and analytical methods employed are described.

AFSC
Arnold AFS Tenn

PREFACE

CONTENTS

ILLUSTRATIONS

APPENDIX

1.0 INTRODUCTION

The need for experimental determinations of the particle size distribution function (PSDF) for particulate matter within the gaseous flow fields encountered in ground-based simulation facilities is a continuing requirement to ensure accuracy of the simulation. The production of supersonic and hypersonic flow fields for aerodynamic simulation purposes normally and necessarily involves the expansion of N_2, air, or other gases which are rarely free of particulate matter whether it be dust, dirt, erosion products, or condensate. The presence of such solid or liquid particulate can result in both a variety of deleterious effects regarding the operation of the facility and its accuracy of simulation and, on rare occasions, a beneficial effect. Considering the latter effect first, the presence of either particulate matter or condensate within the flow field of such a facility is sometimes used to perform so-called unseeded laser velocimeter measurements of the flow speed and velocity of the flow field. Even for this example, the PSDF is of interest so as to be able to quantitatively predict or characterize the gas-particle interaction and, specifically, to determine whether the particle speed is an accurate measure of the gas flow speed.

The common effect of particulate matter in the flow fields of ground-based simulation facilities is one for which performance of the facility is degraded from its design conditions of operation. At best, the particulate mass fraction and PSDF may be such as to result in an insignificant degradation, and even in those cases of observable degradation for which the existence of particles is known, it is rarely possible to determine with any acceptable degree of accuracy both temporal and spatial characteristics of the PSDF and to do so in a nonperturbing manner. In addition to this need for a method to achieve an accurate and extensive characterization of the particulate content of such flow fields it is desirable that the same general approach can be employed to provide routine monitoring of the cleanliness of flow fields whose methods of production necessarily result in the presence of particulate matter. Examples of such facilities are suggested to include not only the more obvious arc-heated flow fields but also those which employ ceramic heaters for which heater erosion is known to occur, facilities which employ either N_2 or air in either continuous or blow-down modes for which strict gas cleanliness is impossible and, of course, all supersonic and hypersonic facilities which operate within the test region either near the saturation point or in a supersaturated condition.

An assessment of the experimental techniques available for particle sizing was performed, and Mie scattering was selected as that technique most likely to satisfy both the then current and anticipated needs of the Arnold Engineering Development Center (AEDC) test facilities, and, consequently, an analytical development program was initiated to determine the limitations of the technique and to ensure the existence of a theoretical base which was adequate for data analysis.

During a recent series of Raman scattering studies of the flow-field properties of the AEDC Von Kármán Gas Dynamics Facility (VKF) arc-heated, hot-shot facility Tunnel F, it became desirable to determine the particle size distribution functions and the mass fraction of particulate matter within the flow field. This facility produces a high-enthalpy flow field of a nominal duration of 130 msec, and both temporal-and spatial-resolved data were desired. Although all inferential evidence concerning particle sizes in this facility indicated a forward scattering geometrical configuration to be most desirable, the exigencies of the measurement program and existing tunnel windows dictated the use of a back-scattering geometrical configuration. Such measurements were achieved using two laser beam injection, detection channels and a novel means of detection of the polarization-resolved scattered intensity as well as the subsequent analysis. This report presents the experimental and analytical methods successfully employed, despite severely unfavorable scattering geometry, in this initial application of Mie scattering at AEDC, and a later report will present in detail the results of the measurements and their implications as applied to VKF Tunnel F.

2.0 MIE SCATTERING AND ITS USE FOR PARTICLE SIZE DISTRIBUTION FUNCTION DETERMINATIONS

The interaction of radiation with material bodies results in, among other processes, the elastic photon-particle scattering process for which the incident wavelength is unchanged by the scattering event, and this process is depicted in Fig. 1. For particles whose diameters (D) are a significant fraction of the wavelength (λ) of the incident radiation such scattering is defined as Mie scattering, which approaches the Rayleigh molecular scattering theory as the ratio D/λ approaches zero (Ref. 1). Restricting consideration to both scattering media and incident fields such that the polarizability is a second-rank tensor, Mie scattering theory is exact for single scattering events, i.e., for the number density of scatterers sufficiently low that multiple scattering events are insignificant.

In addition to the Mie solution for spheres, similar exact solutions exist for scattering of light by cylinders (Ref. 2) and by arbitrary axisymmetric bodies (Ref. 3). Further approximations have been devised to treat scattering by randomly oriented aspherical objects which do not fit into the above categories. For the work reported herein spherical scatterers are assumed.

The Mie theory assumes the medium in which the scatterers are located is isotropic, exclusive of the particles themselves. It is not necessary to consider the medium as being nondispersive nor nonabsorptive, as is sometimes done in textbooks, and the Mie scattering codes we use are based on computational techniques capable of treating scattering with complex indices of refraction for both particles and medium (Refs. 4 and 5). Finally,

it is assumed that the number density of the molecular medium in which the particles are located is sufficiently low that Rayleigh scattering by the surrounding medium is negligible, and it is a simple matter to show that this approximation is justified by all but either extraordinarily particulate-free gas samples or gas samples of extremely high density. Neither of these two cases is of interest to this work, and, consequently, the medium index of refraction is assumed to be unity.

2.1 REVIEW OF MIE SCATTERING THEORY

The interaction of collimated radiation of incident flux I_0 and wavelength λ with a particle of diameter D, located at the coordinate system's origin, is depicted in Fig. 1. The polarization vector of the incident field is assumed to be in the $\hat{x}$ - $\hat{z}$ plane.

The intensity of scattered light received at a point located a distance d from the scatterer is given by the Mie theory for each of the two polarization states by

$$I_{1,2} = \frac{I_0}{(kd)^2} \, i_{1,2}(x,\theta,\eta) \, (\sin^2\phi, \cos^2\phi) \tag{1}$$

where $X = \pi D/\lambda$, $k = 2\pi/\lambda$, $x\eta$ is the particle index of refraction relative to that of the medium, and θ and ϕ are, repectively, the polar angle and azimuthal angle of the spherical coordinate scheme shown in Fig. 1. Figure 2 shows typical variation of i_1 and i_2 with x for copper spheres. The indices 1 and 2 refer, respectively, to the polarization states in which the scattered light electric field vector is perpendicular (1) and parallel (2) to the scattering plane. The angle θ is denoted as the scattering angle. The azimuthal factors $\sin^2\phi$ and $\cos^2\phi$ are associated, respectively, with polarization states 1 (perpendicular) or 2 (parallel).

From Eq. (1) the differential scattering cross section can be inferred to be

$$\frac{d\sigma}{d\Omega} = \frac{i_{1,2}(x,\theta,\eta) \, (\sin^2\phi, \cos^2\phi)}{k^2} \tag{2}$$

If one integrates Eq. 2 over 4π sr for each polarization state and sums the result, the total scattering cross section (σ_T) is obtained. The computer program developed for this work gives the ratio of σ_T and the particle's geometrical cross section $\pi(D/2)^2$, and this ratio is defined as the total scattering efficiency (Q_T). The computer program also yields the total extinction efficiency, which is the total scattering efficiency plus the absorption efficiency. The obvious significance of the extinction efficiency is that it determines the degree of attenuation of the radiation as it passes through the medium containing the scattering particles. If the optical path length along which energy is lost from the incident beam by scattering and absorption is L, the energy flux of transmitted light is

$$\Phi_{Tr} = \Phi_0 \, e^{-\bar{\sigma}_{ext} L \bar{n}} \tag{3}$$

where $\bar{n}$ is the particle number density (all sizes) averaged over the distance L and $\bar{\sigma}_{ext}$ which equals $\overline{\pi Q_{ext}(D/2)^2}$, denotes the average of the extinction cross section over the particle size distribution. Figure 3 shows the variation of $\sigma_{ext}(x)$ with particle size. Consequently, if the particle number density is known, knowledge of the light attenuation permits a type of average particle size $\bar{x}_{ext}$ to be determined. The precise form of the average is difficult to determine, but it is defined as the inverse of the relation

$$\bar{\sigma}_{ext}(\bar{x}_{ext}) = \int_0^\infty \sigma_{ext}(x) \, f(x) \, dx$$

where $f(x)$ is the particle size distribution function.

Since the above described procedure depends on particle number density which is generally unknown, and on obtaining accurate absolute intensity measurements, the procedure is not used directly. Instead, a combination of this procedure with the angular scattering procedures is used, as will be described in a following paragraph, and a formal mathematical deconvolution procedure is applied. Using this combination enables one to infer self-consistent values of average particle size, number density of particles, and estimates of particle size distribution by mole fractions in each of as many as four size bins (in the case of this experiment) spanning the size range of interest. Considering angular Mie scattering and assuming that the solid angle $(\Delta\Omega)$ is subtended by a detector located at the spherical polar coordinates (d, θ_s, ϕ_s) the scattered flux received by the detector is given by

$$\frac{\Phi_{1,2}(\theta_s, \phi_s)}{\Phi_0} = \frac{n\ell}{k^2} \int_{\phi_s - \Delta\phi/2}^{\phi_s + \Delta\phi/2} \int_{\theta_s - \Delta\theta/2}^{\theta_s + \Delta\theta/2} i_{1,2}(x, \theta, \eta)(\sin^2\phi, \cos^2\phi) \, d\Omega \qquad (4)$$

where $d\Omega = \sin\theta \, d\theta \, d\phi$, ℓ = length of the scattering volume, and the ordering of the subscripts 1 and 2 and the parenthetical factors $\sin^2\phi$, $\cos^2\phi$ is to be maintained.

2.2 TECHNIQUES FOR AVERAGE PARTICLE SIZE DETERMINATIONS

For the application of Mie scattering for the determination of particle sizes in aerodynamic simulation facilities it is the usual case that the local total number density of particulate as well as the chemical identity of the scatterer are not known. For this reason and, also, to eliminate the necessity for corrections required for laser power fluctuations, the approach taken in this effort was to obtain ratios of various experimentally determined quantities, and the Angular/Extinction ratio* technique is an example of such a procedure. In this method measurements are performed for the extinction of the incident radiation as well as for the power or photon rate scattered into detectors located at various

---

*This ratio is related to a quantity denoted as a phase function by astrophysicists and radiative transport theorists.

scattering angles. It is assumed that the particles responsible for the extinction and scattering processes are the same. Using the transmitted power measurements, one obtains the quantity $\langle n\sigma_{ext}\ell \rangle$, where $\langle n\sigma_{ext}\ell \rangle$ represents an average of the quantity $n\sigma_{ext}\ell$ over the length L of the scattering medium. The additional approximation is made

$$\langle n\sigma_{ext}\ell \rangle \simeq \bar{n}\,\bar{\sigma}_{ext}L$$

where $\bar{n}$ is the average number density of particles over the distance L of the scattering medium, intervening between the points of laser beam injection and transmission detector. From the angular scattering measurement, assuming the detector to be located at scattering angle θ_s, one obtains the quantity $n\ell\bar{\sigma}_{1,2}(\bar{x}_s,\theta_s)$

where

$$\bar{\sigma}_{1,2}(\bar{x}_s,\theta_s) = \int_0^\infty \sigma_{1,2}(x,\theta_s)\,f(x)\,dx$$

and n is the number density of particles in the cylindrical scattering volume V_s, with length ℓ. It is assumed that the ratio $\bar{n}L/n\ell$ can be estimated or measured. Thus, the experimental quantity

$$-\left(\frac{\overline{\Phi}_{1,2}}{\Phi_o}\right)\frac{\bar{n}L}{n\ell}\bigg/ \ell n\left(\frac{\Phi_{Tr}}{\Phi_o}\right) = \bar{\sigma}_{1,2}(\theta,\bar{x})\bigg/\bar{\sigma}_{ext}(\bar{x}) \qquad (5)$$

can be compared with calculations of $\sigma_{1,2}(x,\theta_s)/\sigma_{ext}(x)$ versus x. Figure 4 shows as a function of size parameter x this calculated cross section ratio for one scattering angle and one state of polarization. From Fig. 4 it is seen that such an experimental measurement can yield an estimate of the range of particle size parameter $\bar{x}_s$ or average particle diameter $\overline{D}_s$, consistent with the experimental results. It is obvious that this method, as exemplified by the use of Fig. 4, can quite conceivably result in a nonunique particle size parameter x; e.g., if the experimental angular/extinction ratio were found to be, say, 0.12, the range of the resulting value of x is seen from Fig. 4 to be $0.5 \lesssim x \lesssim 2.4$. Consequently, it is desired to provide additional measures for $\overline{D}_s$ even though four plots to the type of Fig. 4 are used, corresponding to measurements at two scattering angles and in both polorization states.

An additional procedure for providing a separate and distinct determination of an average particle size parameter involves the formation of linear combinations of ratios of the angular scattered intensities in two polarization states. One such combination, defined to be the degree of polarization $P(\theta_s,x)$ is

$$P_{(\theta_s,x)} = \frac{\left[i_1(\theta_s,x)\right] - \left[i_2(\theta_s,x)\right]}{i_1(\theta_s,x) + \left[i_2(\theta_s,x)\right]} \qquad (6)$$

where

$$\left[i_{1,2}(\theta_s, x)\right] = \int_{\theta_s - \Delta\theta/2}^{\theta_s + \Delta\theta/2} i_{1,2}(x, \theta, \eta) \sin\theta\, d\theta$$

and $P(\theta_x, x)$ ranges from 0 for the unpolarized case to ± 1 for the completely polarized case.

The variation of $P(\theta_s, x)$ with size parameter x is shown in Fig. 5 for the case θ_s = 146.5 deg. For a polydisperse sample of PSDF, $f(x)$, one can define an average size parameter $\bar{x}$ by the relation

$$\bar{P}_{(\theta_s, \bar{x})} = \frac{\int_0^\infty \left[i_1(\theta_s, x)\right] - \left[i_2(\theta_s, x)\right] f(x)\, dx}{\int_0^\infty \left[i_1(\theta_s, x)\right] + \left[i_2(\theta_s, x)\right] f(x)\, dx} \tag{7a}$$

$$= \frac{\bar{\Phi}_1(\theta_s) - \bar{\Phi}_2(\theta_s)}{\bar{\Phi}_1(\theta_s) + \bar{\Phi}_2(\theta_s)} \tag{7b}$$

Consequently, as many estimates of $\bar{x}$ are provided as there are detectors at the various scattering angles, θ_s.

It is quite obvious that the resulting value of $\bar{x}$ determined by either the first method or any one detector using the second method is decidedly nonunique as a result of the absence of monotonicity in the variation of the dependent function with x. However, it was found that a combination of both the first and second methods, the latter employing two detectors, was sufficient to reduce the uncertainty in $\bar{x}$ and $\bar{D}$ to acceptable levels.

2.3 DECONVOLUTION OF SIZE DISTRIBUTION FUNCTION

Assuming the polydisperse particulate sample to be described by the PSDF, $f(x)$, the energy flux $\Phi_{1,2}$ detected at the scattering angle θ_s is given by

$$\bar{\Phi}_{1,2}(\theta_s) = \int_0^{x_{max}} \Phi_{1,2}(\theta_s, x) f(x)\, dx \tag{8}$$

where x_{max} is the largest size parameter of significance for the problem at hand. It is obviously of interest to deconvolve Eq. (8) to extract the desired PSDF, $f(x)$, and such a process is the formal inversion of Eq. (8). Prior to a discussion of this inversion procedure

it is worthwhile to review the general nomenclature of integral equations. The following equation

$$\hat{\phi}(x) = \hat{f}(x) + \lambda \int_a^b K(x,\xi) \, \hat{\phi}(\xi) \, d\xi \tag{9a}$$

is known as either the Fredholm equation or an integral equation of the second kind. In Eq. (9a) and the following Eqs. (9) it is assumed that ξ and x are real continuous variables and the functions $\hat{\phi}(x)$, $\hat{f}(x)$ and $K(x,\xi)$ satisfy the appropriate mathematical requirements of continuity, finiteness, and integrability as necessary to ensure meaning for the equation. In Eq. (9a) $K(x,\xi)$ is defined to be the kernel of the equation, and, if $K(x,\xi) = K(\xi,x)$, the kernel is said to be symmetric. Further, if $\hat{f}(x)$ equals zero one has a homogeneous integral equation

$$\hat{\phi}(x) = \lambda \int_a^b K(x,\xi) \, \hat{\phi}(\xi) \, d\xi \tag{9b}$$

and, as in Eq. (9a), λ is in general a complex constant parameter. Finally, the integral equation of the first kind is defined by

$$\hat{f}(x) = \lambda \int_a^b K(x,\xi) \, \phi(\xi) \, d\xi \tag{9c}$$

and, as in Eqs. (9a) and (9b), a and b are assumed to be the real number limits of the integrals.

It is seen by comparison of Eqs. (8) and (9c) that the inversion or deconvolution for determining $f(x)$ is formally equivalent to a solution of an integral equation (Fredholm) of the first kind. Further, one can easily see that if ratios of the scattered intensity values or, equivalently, the scattered energy flux values are used the type of equation to be inverted is of the form

$$\overline{\Phi}_{1,2}(\theta_{s1})/\overline{\Phi}_{1,2}(\theta_{s2}) = \frac{\displaystyle\int_o^{x_{max}} \Phi_{1,2}(\theta_{s1},x) \, f(x) \, dx}{\displaystyle\int_o^{x_{max}} \Phi_{1,2}(\theta_{s2},x) \, f(x) \, dx} \tag{10}$$

which is easily shown to be an integral equation of the first kind.

The denominator of the right-hand side of Eq. (1) can, of course, be considered as a normalization constant. However, for iterative solution procedures for f(x) its value will vary as f(x) varies, thereby complicating somewhat the iterative procedure. Consequently, it is desirable to select both a value θ_{ref} for θ_{s2} and a combination function of $\Phi_{1,2}(\theta_{ref},x)$, say $\widetilde{\approx}$ $[\Phi_{1,2}(\theta_{ref},x)]$ such that $\widetilde{\approx}$ exhibits an insignificant variation with x. If this is approximately true one sees that

$$\widetilde{\approx}\,(\theta_{ref}) = \int_0^{x_{max}} \widetilde{\approx}\big[\Phi_{1,2}(\theta_{ref},x)\big]\,f(x)\,dx \doteq \widetilde{\approx}\big[\Phi_{1,2}(\theta_{ref},\bar{x})\big] \tag{11}$$

since

$$\int_0^{x_{max}} f(x)\,dx = 1.$$

Therefore, in this approximation, the value of $\widetilde{\approx}[\Phi_{1,2}(\theta_{ref},x)]$ assumes the role of a normalization constant, which simplifies the iteration process.

For the sizing of particles of the range of diameters anticipated for the present application, VKF Tunnel F, the desired configuration of scattering was estimated to be for the scattering angle range $0 \leq \theta \lesssim 40$ deg and for $\theta_{ref} = 90$ deg; also $\widetilde{\approx}$ was anticipated to be the sum of $\overline{\Phi}_1$ and $\overline{\Phi}_2$ at θ_{ref}. However, as mentioned previously, a back-scattering configuration was required by other constraints for this application and $\widetilde{\approx}$ was taken to be the sum of the scattered flux values from the two angular detectors, each summed over both polarization states; i.e.,

$$\widetilde{\approx} = \widetilde{\approx}_1(\theta_1) + \widetilde{\approx}_2(\theta_1) + \widetilde{\approx}_1(\theta_2) + \widetilde{\approx}_2(\theta_2) \tag{12}$$

where θ_1 and θ_2 were the scattering angles.

The set of input data for the PSDF deconvolution scheme is taken to be the 4-component vector

$$g_1 = \Phi_1(\theta_1)/\widetilde{\approx}$$

$$g_2 = \Phi_1(\theta_2)/\widetilde{\approx}$$

$$g_3 = \Phi_2(\theta_1)/\widetilde{\approx} \tag{13}$$

$$g_4 = \Phi_2(\theta_2)/\widetilde{\approx}$$

The deconvolution scheme is described in Appendix A and consists of a matrix inversion procedure using the symmetric matrix $\underline{M} = \underline{Q}^T \underline{Q}$, where the scattering kernels $\underline{Q}$ are defined to be

$$Q_{1j} = A_{1j} \big| R \qquad Q_{3j} = B_{1j} \big| R$$

$$Q_{2j} = A_{2j} \big| R \qquad Q_{4j} = B_{2j} \big| R \tag{14}$$

where

$$R = (1/N) \sum_{j=1}^{N} (A_{1j} - A_{2j} + B_{1j} + B_{2j})$$

and N is the number of size bins to be used.

The quadratures A_{ij} and B_{ij} are obtained by numerical integration of the Mie functions over the size bins

$$A_{ij} = \int_{x_{j-1}}^{x_{s}} \left[i_1(\theta_i,x) \right] \frac{dx}{(x_j - x_{j-1})} \tag{15}$$

and

$$B_{ij} = \int_{x_{j-1}}^{x_{j}} \left[i_2(\theta_i,x) \right] \frac{dx}{(x_j - x_{j-1})}$$

The output of the deconvolution procedure is a histogram of mole fractions in preselected equal size bins. These mole fractions are related to the actual continuous and unknown size distribution function by $F_j = \int_{x_{j-1}}^{x_j} F(x)dx$, and the size range x_j-x_{j-1} defines a size bin.

Because the deconvolution procedure is based on properties of the symmetric scattering kernel matrix $\underline{M} = \underline{Q}^T \underline{Q}$, the deconvolved mole fractions represent a least squares solution. Consequently, the requirement that the number of size bins equal the number of independent angular scattering input ratios is removed.

3.0 EXPERIMENTAL METHOD

3.1 EXPERIMENTAL APPARATUS

The experimental arrangement and apparatus employed for this study are shown in Fig. 6 and it is seen that the laser beam is injected diagonally across the flow field, using

existing Tunnel F ports, and scattering detectors are located at the scattering angles of 146.5 and 161.9 deg. The laser source used was an Ar-Ion Coherent Radiation Model CR-5, source which was operated at 514.5 nm with an average output power of 0.62w as measured with a Coherent Radiation Model 210 power meter. The laser-beam-transmitted power across the tunnel flow was measured with a Coherent Radiation Model 212 power meter, and the transmission signal was displayed on a Tektronix Model 7633 oscilloscope and photographic recording was used. Since the level of visible fluorescence from the flow field was unknown prior to entry, provision was made for electronically modulating the laser output power using a signal generator operated at nominal 1,000 Hz. From Fig. 6 it is seen that the laser beam traversed the 54.5-in.-diam tunnel along a window-to-window, line-of-sight distance of 78.4 in. (199 cm).

Once again, because of our lack of knowledge of the flow-field fluorescence levels, spectrometers were employed in the detection of the scattered signal to achieve spectral isolation. These two spectrometers used were 0.75-m and 0.25-m instruments, respectively, and RCA 31034A photomultiplier tubes were used for detection. Data processing was accomplished with routine photon counting instrumentation, and data recording for the two channels was accomplished with dual-beam oscilloscopes.

The novel feature of the experimental system was the method employed to achieve resolution of the data in both time and polarization. The collected scattered radiation was passed through chopper wheels shown in Fig. 7, and the modulation frequency was such as to provide a nominal time resolution of 10 msec. To achieve polarization resolution, alternate slits in the chopper were outfitted with polarizer material, and the polarization direction of the successive slits was crossed. Each third slit was blank to provide an unpolarized signal as well as a time mark reference. Figure 7 shows a sketch of this arrangement. Consequently, time-resolved measurements of $\overline{\Phi}_1(\theta)$, $\overline{\Phi}_2(\theta)$ and $\overline{\Phi}_1(\theta)$ + $\overline{\Phi}_2(\theta)$ could be achieved. Finally, a polarization rotator was located in the laser injection optical train to orient the input electric field such that $\phi = 45$ deg, the importance of which is seen from Eq. (1).

3.2 CALIBRATION AND OPERATION

The system sensitivity was determined by performing Rayleigh scattering measurements in air both before and after tunnel firings. Depolarization measurements were performed to ensure the absence of particulate scattering in these calibrations, and the known Rayleigh cross sections of N_2, O_2, and CO_2 as well as the air composition were used to determine quantitatively the system sensitivity. Further, the solid angles subtended by the detectors at the scattering volume were accurately determined to enable the conversion from scattered intensity to power flux.

14

The firing of the tunnel provided a trigger source for the instrumentation channels, and the calibrated oscilloscope sweep rate as well as the chopper modulation frequency provided time-mark references. Data reduction was effected in a routine manner, linearity of performance of the overall system having been ensured.

4.0 RESULTS

4.1 AVERAGE SIZE DETERMINATION

Using the previously described techniques, the measured flux-intensity ratios are

$$\frac{\Phi_1(\theta_1)}{\Phi_0} = 1.02 \times 10^{-7} \pm 5\%$$

$$\Phi_2(\theta_1)/\Phi_0 = 8.10 \times 10^{-8} \pm 3.6\%$$

$$\Phi_1(\theta_2)/\Phi_0 = 2.70 \times 10^{-7} \pm 6\%$$

$$\Phi_2(\theta_2)/\Phi_0 = 1.68 \times 10^{-7} \pm 4.2\%$$

and

$$\Phi_{Tr}/\Phi_0 = 0.96$$

where $\theta_1 = 146.5$ deg and $\theta_2 = 161.9$ deg. The imprecision of Φ_{Tr}/Φ_0 is estimated to be negligible, particularly in view of the fact that $\ln(\Phi_{Tr}/\Phi_0)$ is the quantity of interest.

Using these raw data, the following parameters are computed for use in the average size analysis procedures:

Degree of Polarization

$$P(\theta_1) = 0.114 \pm 0.030 \qquad P(\theta_2) = 0.232 \pm 0.035$$

Angular/Extinction Ratios

$$R_1(\theta_1) = 0.065 \pm 0.003 \qquad R_2(\theta_1) = 0.052 \pm 0.002$$

$$R_1(\theta_2) = 0.116 \pm 0.007 \qquad R_2(\theta_2) = 0.072 \pm 0.003$$

for

$$\overline{L} = \frac{48.0 \text{ in.}}{\cos(18.1^\circ)}$$

and

$$R_1(\theta_1) = 0.069 \pm 0.003 \qquad R_2(\theta_1) = 0.055 \pm 0.002$$

$$R_1(\theta_2) = 0.123 \pm 0.007 \qquad R_2(\theta_2) = 0.077 \pm 0.003$$

for

$$\overline{L} = \frac{51.0 \text{ in.}}{\cos(18.1°)}$$

The first value of $\overline{L}$ (representing a lower limit on the distance over which scattering and absorption occur) is the nozzle exit diameter, corrected for the obliquity of the laser beam. The second value of $\overline{L}$ represents the obliquity-corrected expanded flow dimension at the observation station and was calculated using a method of characteristics technique.

The computer simulation of scattering by various size distributions of the form

$$f(x) = \frac{C^{N+1}}{N!} x^N e^{-Cx}$$

indicates that the angular/extinction technique is capable of average diameter determination with perhaps $\pm10\%$ uncertainty if $\overline{L}$ is known accurately. In the present experiment, knowledge of $\overline{L}$ is the limiting factor in determining the average diameter accurately. The range of angular/extinction ratios associated with the upper and lower limits on $\overline{L}$ has considerable overlap with the range of ratio values obtained using the lower limit for $\overline{L}$ and the 2-σ error bars of the experimental data. Consequently, this uncertainty in $\overline{L}$ is within the imprecision of the measurement method.

Figures 8 and 9 show the computed degree of polarization with the nominal experimental values and error brackets (1 standard deviation) superimposed. The same type of graph was computed for iron particles and the results showed that iron particles were not the major contributor to the observed scattering. Finally, the computed angular/extinction ratios are shown in Figs. 10 through 13 along with the measured values of these parameters. From Figs. 8 through 13 it can be seen that the only average particle diameter $\overline{D}$ which is consistent with the experimental data, assuming 1-σ error limits and for $\overline{L} = (51.0/\cos 18.1°)$, in. is $0.7 \leqslant \overline{D} \leqslant 0.9$ μm. A similar analysis eliminated tungsten, water, and condensed nitrogen from consideration as single species sources of scattering. Multiple species combinations are beyond the scope of this report, but will be considered in future analyses.

4.2 SIZE DISTRIBUTION DECONVOLUTION

Using the average diameter range $0.7 \leq \bar{D} \leq 0.9$ μm one can directly determine the two bin size histogram, using the following relations:

$$F_1 = \frac{\bar{D} - D_{12}}{D_{01} - D_{12}} \qquad \text{and} \qquad F_2 = \frac{\bar{D} - D_{01}}{D_{01} - D_{12}}$$

where D_{01} and D_{12} are, respectively, the mean diameters corresponding to the first and the second size bins, and F_1 and F_2 are, respectively, the particle mole fractions in the first and second size bins. Using size bins encompassing the range of diameters 0 to 1.0 μm and 1.0 μm to 2.0 μm, for example, we obtain $F_1 = 0.8$ and $F_2 = 0.2$ for $\bar{D} = 0.7$ μm and $F_1 = 0.6$ and $F_2 = 0.4$ for $\bar{D} = 0.9$ μm. Thus, it is estimated that 60 to 80 percent of the particles have diameters less than 1.0 μm.

More sizing detail than the above can be obtained from the multibin deconvolution procedure. Computer simulation of scattering from polydisperse size distributions of the form

$$F(x) = \frac{C^{N+1}}{N!} e^{-Cx}$$

show that very accurate deconvolutions are obtained by the use of a number of forward scattering detector channels and a 90-deg scattering reference signal, as was mentioned in a previous section. Shown in Fig. 14 is an example of such a deconvolution of simulated measurements for which five simulated forward scattering angular measurements (0 to 40 deg) were used along with only one polarization state. Using three forward and two backward angles with polarization states, we have recently achieved accurate deconvolution into twice as many size bins.

As stated previously, the Tunnel F scattering geometry is less than ideal. As a consequence, the deconvolution procedure has necessarily been modified. Deconvolution of simulated polydispersions has shown that with these modifications to the deconvolution technique, the computed mole fraction histograms are less sensitive to the input data than they are to the average diameter. Thus, in the context of the Tunnel F experiment, the smooth sizing procedure becomes a sophisticated technique for varying the mole fraction distribution in a systematic fashion until the computed average diameter agrees with the average diameter determined as described in the previous section.

Figure 15 shows a comparison of the deconvolved Tunnel F measurements with a simulated polydispersion having a similar average diameter. Although not shown, comparison with a similar polydispersion which peaked at the same diameter but had a smaller average diameter (by a factor of 1.5) indicated that adjusting the smoothing parameter until correct average diameters are obtained in the deconvolution procedure

yields histograms whose largest mole fractions are correct to at least 10 to 15 percent, but whose smallest mole fractions (on the tail of the distribution) are unreliable. In fact, when the true mole fraction is less than one percent, the computed result can even go negative.

The inputs for the deconvolution of the measured light scattering data are

$$g_1 = 0.164 \qquad g_3 = 0.131$$

$$g_2 = 0.434 \qquad g_4 = 0.271$$

When the deconvolution was undertaken with zero smoothing, negative mole fractions were obtained in two of the bins and the computed average diameter was an order of magnitude too small. Negative mole fractions did not disappear until the smoothing parameter (starting from zero) reached 0.0027. yielding an average diameter of 0.52 μm and a computed error parameter of the same order of magnitude as the experimental value. The mole fraction histogram corresponding to these values is given below.

Mole Fraction	Bin Diameter, μm
0.556	0.008 - 0.5
0.332	0.5 - 0.99
0.109	0.9 - 1.48
0.002	1.48 - 1.97

When the smoothing process is continued until the computed average diameter agrees with the previously determined range of values one obtains the histogram shown in Fig. 15 and tabulated below (for smoothing parameter = 0.0219).

Mole Fraction	Bin Diameter, μm
0.45	0.008 - 0.5
0.31	0.5 - 0.99
0.17	0.99 - 1.48
0.06	1.48 - 1.97

and $\bar{D} = 0.67$ μm.

The analogous 3-bin histogram is:

Mole Fraction	Bin Diameter, μm
0.58	0.008 - 0.66
0.32	0.66 - 1.32
0.10	1.32 - 1.97

and $\overline{D}$ = 0.67 μm.

Two-bin results with larger size range are

Mole Fraction	Bin Diameter, μm
0.97	0.008 - 1.32
0.03	1.32 - 2.63

and $\overline{D}$ = 0.7 μm; and

0.82	0.008 - 1.32 μm
0.18	1.32 - 2.63 μm

and $\overline{D}$ = 0.9 μm.

5.0 CONCLUSIONS AND RECOMMENDATIONS

Using the results of the previous section, it is of interest to obtain an order of magnitude estimate of the average particulate mass fraction a_p which is defined to be the ratio of the particulate mass density ρ_p and the sum of the gas density (ρ_g) and ρ_p. For this computation the particles are assumed to be copper spheres of density ρ_s = 8.89 gm/cc and the flow-field condition is assumed to be ρ_g = 2.12 x 10^{-5} gm/cc, T_∞ = 60 K, and v_∞ = 2.5 x 10^5 cm/s, where T_∞ and v_∞ are the flow-field kinetic temperature and flow speed, respectively. Using the transmission relation and assuming uniform particulate density across the flow field one can easily show that

$$\rho_p/\rho_g = \pi\rho_s \cdot \overline{D}^3 \cdot \ln(1/\tau)/6\rho_g \cdot \sigma_D \cdot L$$

where $\overline{D}$ is the mean particle diameter, τ is the transmission factor, σ_D is the extinction cross section for a particle of diameter $\overline{D}$, and L is the transmission length.

Using the assumed values one finds

$$\rho_p/\rho_g = 66.3 \ (\overline{D}^3/\sigma_D)$$

and from Fig. 3 one finds that for $\overline{D} = 0.8\,\mu m$, $\sigma_D = 1.5 \times 10^{-8}$ cm^2. Consequently,

$$\rho_p/\rho_g \simeq 2.3 \times 10^{-3}$$

which results in

$$\alpha_p = \rho_p/(\rho_p + \rho_g) = \left(\frac{\rho_p}{\rho_g}\right)\Big/\left(1 + \frac{\rho_p}{\rho_g}\right) \simeq 2.3 \times 10^{-3}.$$

Therefore, the approximate particulate mass fraction for this case is 2.3 x 10^{-3}.

It is of interest to recall the imprecision limits of $\overline{D}$: $\overline{D} = 0.8 \pm 0.1\,\mu m$. Translating this uncertainty in $\overline{D}$ into a corresponding uncertainty in α_p, one finds

$$\alpha_p \simeq (2.3 \pm \begin{smallmatrix} 0.3 \\ 0.4 \end{smallmatrix}) \times 10^{-3}$$

showing the imprecision in α_p to be on the order of ± 10 percent.

Although the Reynolds number for the particle-gas flow field cannot be simply computed, one can estimate the likelihood of significant particle lag. The characteristic time τ_v for particle lag can be defined as (Ref. 6).

$$\tau_v = \overline{D}\rho_s/18\nu$$

where ν is the gas viscosity which is approximated by $\nu \cong 4.5 \times 10^{-5}$ cgs. From this equation for τ_v, one finds for $\overline{D} = 0.8\,\mu m$.

$$\tau_v \sim 10^{-4} \text{ sec.}$$

Now, a characteristic flow time is assumed to be crudely given by the quantity

$$\tau_F \sim \Delta L/(v_{th} - v_\infty)$$

where v_{th} is the flow speed at the nozzle throat, v_∞ is the free-stream speed, assumed to be acquired at the nozzle exit plane, and ΔL is the length of the nozzle from throat to exit. Using reasonable values for ΔL, v_{th} and v_∞, one finds

$$\tau_F \sim 5 \times 10^{-3} \text{ sec.}$$

Therefore,

$$\tau_v \sim 0\,(100 \times \tau_v)$$

and one expects that particle lag effects will not be significant since the flow-field speed is changing more slowly than the speed with which the particle can relax or be

accommodated to that change. Consequently, one expects that the particle flow speed $v_p \simeq v_\infty$ and the Reynolds number

$$Re = \rho_s \cdot \overline{D} \left| v_\infty - v_p \right| / \nu$$

will be quite small because of the near-equality of v_p and v_∞.

Now, one can make use of this result to determine an order of magnitude estimate of the total particle mass contained within the flow field of an estimated usable run time of 130 msec. Assuming $v_p = v_\infty$, temporally uniform mass flux, and that the circular cross-sectional area of the flow field is 1.3×10^4 cm^2, corresponding to a flow diameter of $\simeq 130$ cm, one finds the total mass (Δm) within the flow, after the establishment of the flow, to be

$$\Delta m \sim 20 \text{ gm.}$$

That the preceding estimates are at best crude order of magnitude computations is emphasized by the neglect of the transition of the particle flow from a continuum environment to a free molecular condition in the test section where the particle Knudsen number is estimated to be on the order of 100. This transition is estimated to occur between the nozzle throat and exit plane and should be considered in more detail for more accurate estimates.

Other quantitative results of interest include the particle number density. Again, using a particle of mean diameter $\overline{D} = 0.8$ μm for computations one finds the mass per particle to be 2.4×10^{-12} gm and a particle number density (n_p) to be

$$n_p \simeq 2 \times 10^4 \text{ cc}^{-1}.$$

Further, the specific volume ($\tilde{v}_p$) is found to be

$$\tilde{v}_p = 1/n_p = 4.9 \times 10^{-5} \text{ cc}$$

so that a mean distance between particles can be found to be

$$(1/n_p)^{1/3} = \tilde{v}_p^{1/3} = 3.6 \times 10^{-2} \text{ cm.}$$

Finally, using the well-known criterion for incoherent scattering

$$2k \cdot \sin(\theta/2) \cdot \tilde{v}^{1/3} \gg 1$$

one finds for this measurement

$$2k \sin(\theta/2) \tilde{v}^{1/3} \sim 10^4 \gg 1.$$

Therefore, the scattering process is definitely incoherent as anticipated.

In conclusion, this report has demonstrated both experimental and analytical techniques which provide information concerning the particulate mass fraction in the free stream of an arc-heated hypersonic flow facility. Specifically, an experimental technique has been demonstrated which has the capability of obtaining time-resolved particle size distribution functions, and the time resolution of this work was on the order of 10 msec, a value which can be substantially decreased, if desired. Further, a novel method of measuring in short times both states of polarization of the scattered radiation has been demonstrated along with a method of analyzing such results for the disadvantageous geometry required for the experimental measurements. Additionally, such results have yielded polydisperse particle size distribution functions, mean particle diameter, an estimate of the particulate mass fraction and number density and the total mass of particulate within the usable facility run-time. Finally, the data presented here represent only a small portion of the flow time of one tunnel shot. Obviously, the additional acquired data will allow a presentation of the time-dependent particle size distribution function as well as the just-mentioned mean particle parameters.

REFERENCES

1. Mie, G., Annalen der Physik. Vol. 25, 1908, pp. 377-445.

2. Kerker, M., The Scattering of Light and Other Electromagnetic Radiation. Academic Press, New York, 1969, pp. 255-306.

3. Barber, P. and Yeh, C., "Scattering of Electromagnetic Waves by Arbitrary Shaped Dielectric Bodies." Applied Optics, Vol. 14, 1975, pp. 2864-2872.

4. Mundy, W. C., Roux, J. A., and Smith, A. M. "Mie Scattering by Spheres in an Absorbing Medium." Journal of the Optical Society of America, Vol. 64, 1974, pp. 1593-1597.

5. Dave, J. V. "Subroutines for Computing the Parameters of the Electromagnetic Radiation Scattered by a Sphere." Report No. 320 3237, IBM Scientific Center, Palo Alto, California, May 1968.

6. Rudinger, G. "Relaxation in Gas-Particle Flow." Nonequilibrium Flows, ed. P. Wegener, Marcel Dekker, Inc., New York, 1969, pp. 119-161.
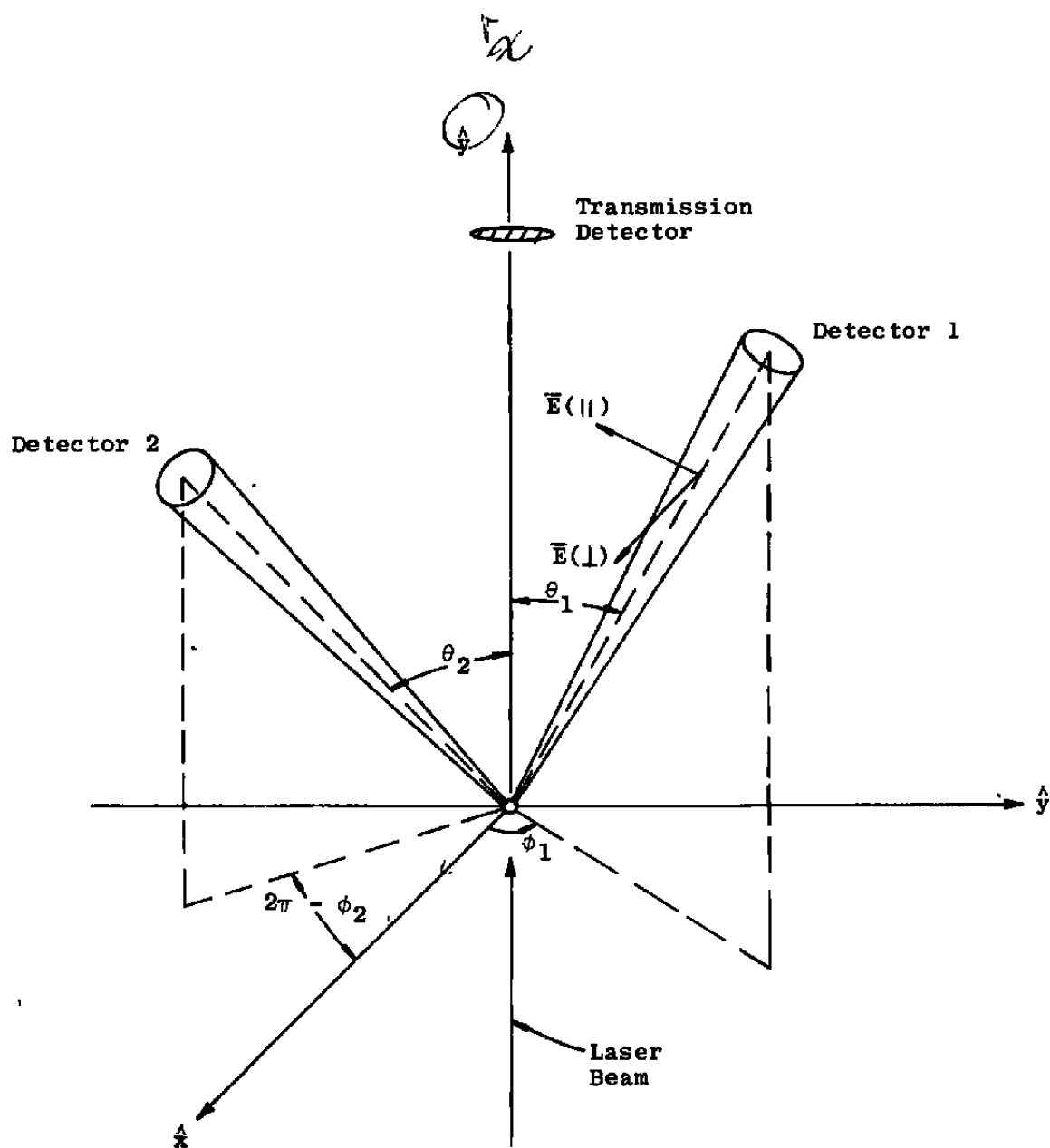
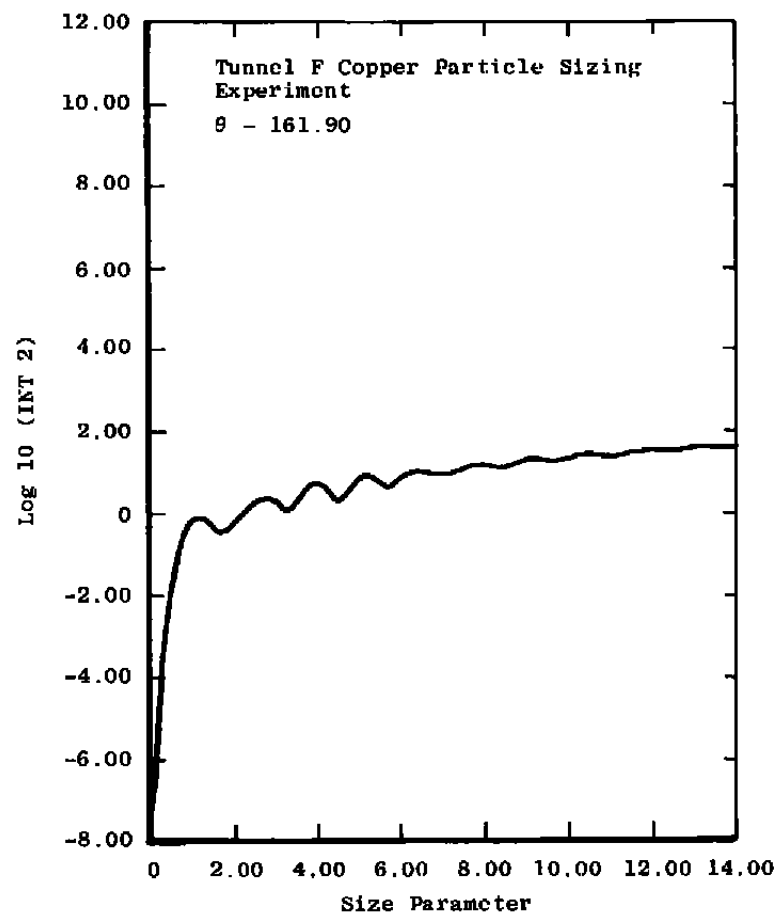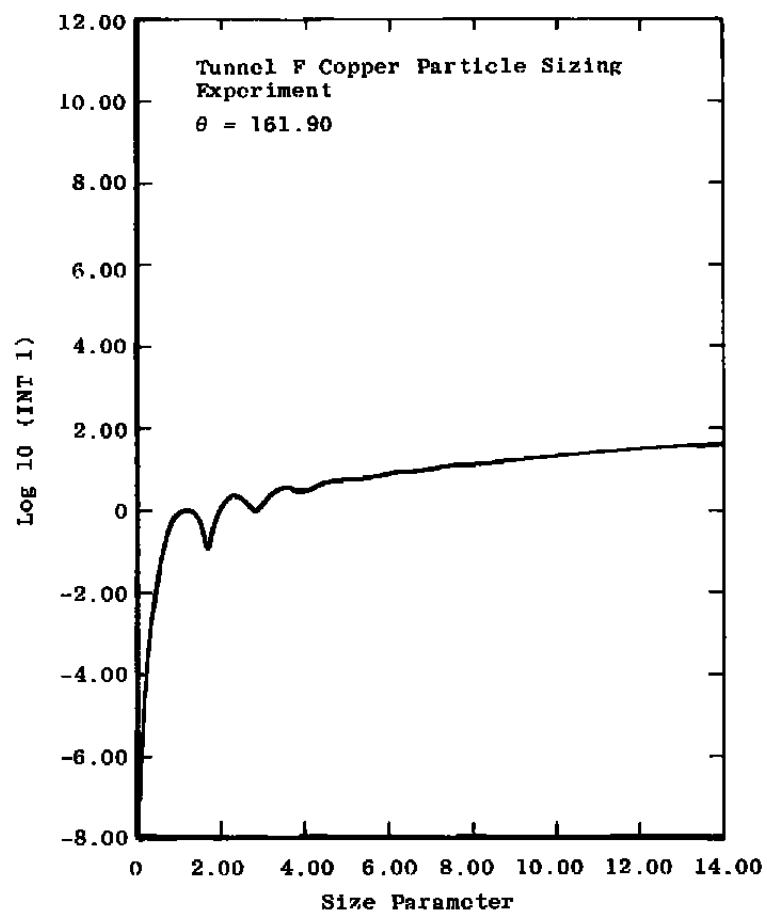**Figure 1. Mie scattering experimental configuration.**

Figure 2. Size dependence of Mie intensity functions in geometry
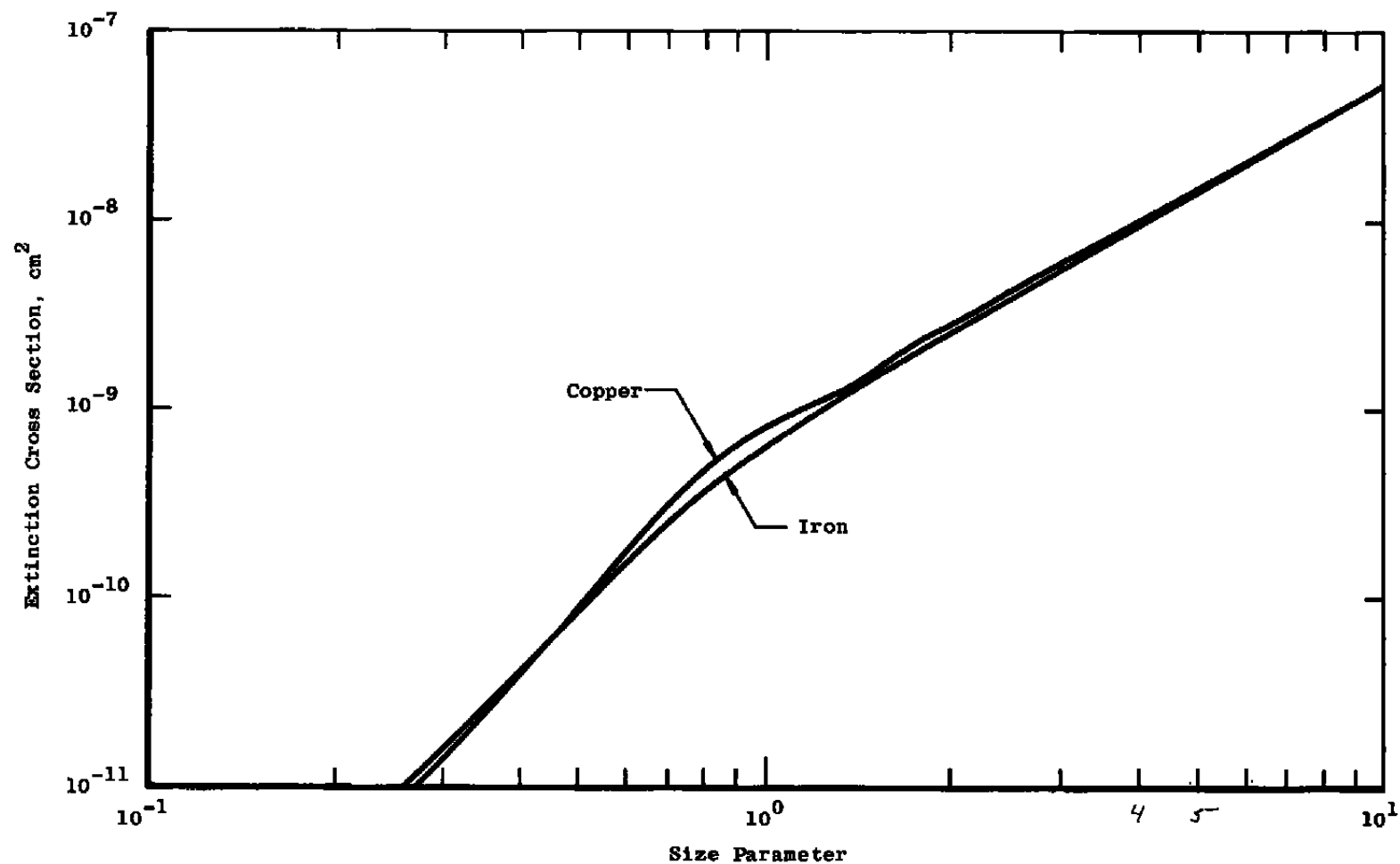of Fig. 1.

Figure 3. Variation of extinction cross section with particle diameter for copper and for iron.

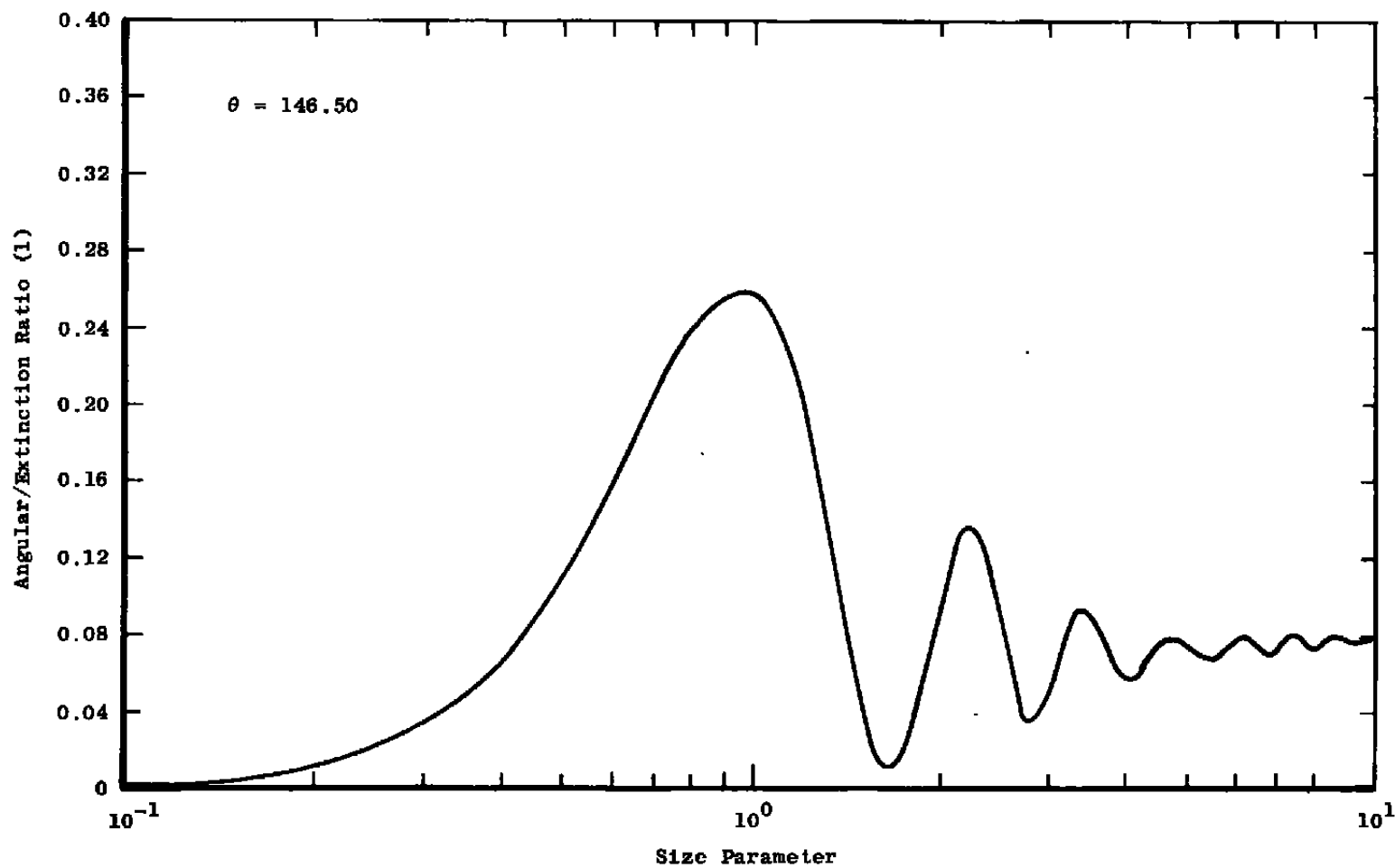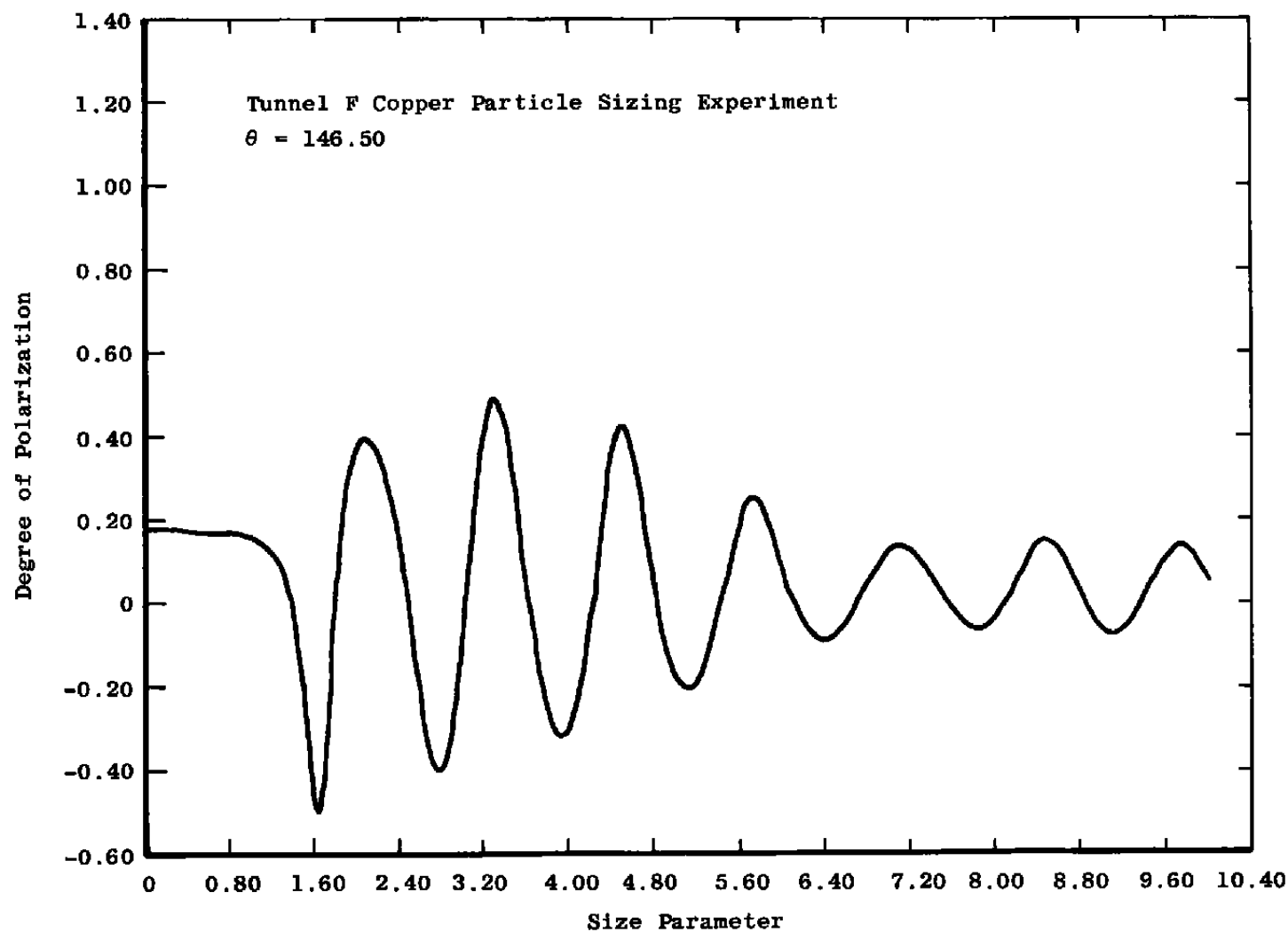Figure 4. Typical angular/extinction ratio plot.

Figure 5. Typical degree of polarization plot.

Transmission Monitor

Dump Adapter

146.5   161.9

Flow ⟹   ₵ Tunnel F

Solid Angles Subtended   2.65 deg   6.60 deg
by Each Spectrometer
Optical Train

3/4-meter – Ω_c = 1.69 x 10^{-3} sr

1/4-meter – Ω_c = 1.05 x 10^{-2} sr

⊢——⊣ 10 in.

C – Chopper

C   PMT

Fresnel
Lenses

C

1/4-
m

CR-5 Ar-Ion
Laser

3/4-m

PMT

Table

Power Supply
Modulation
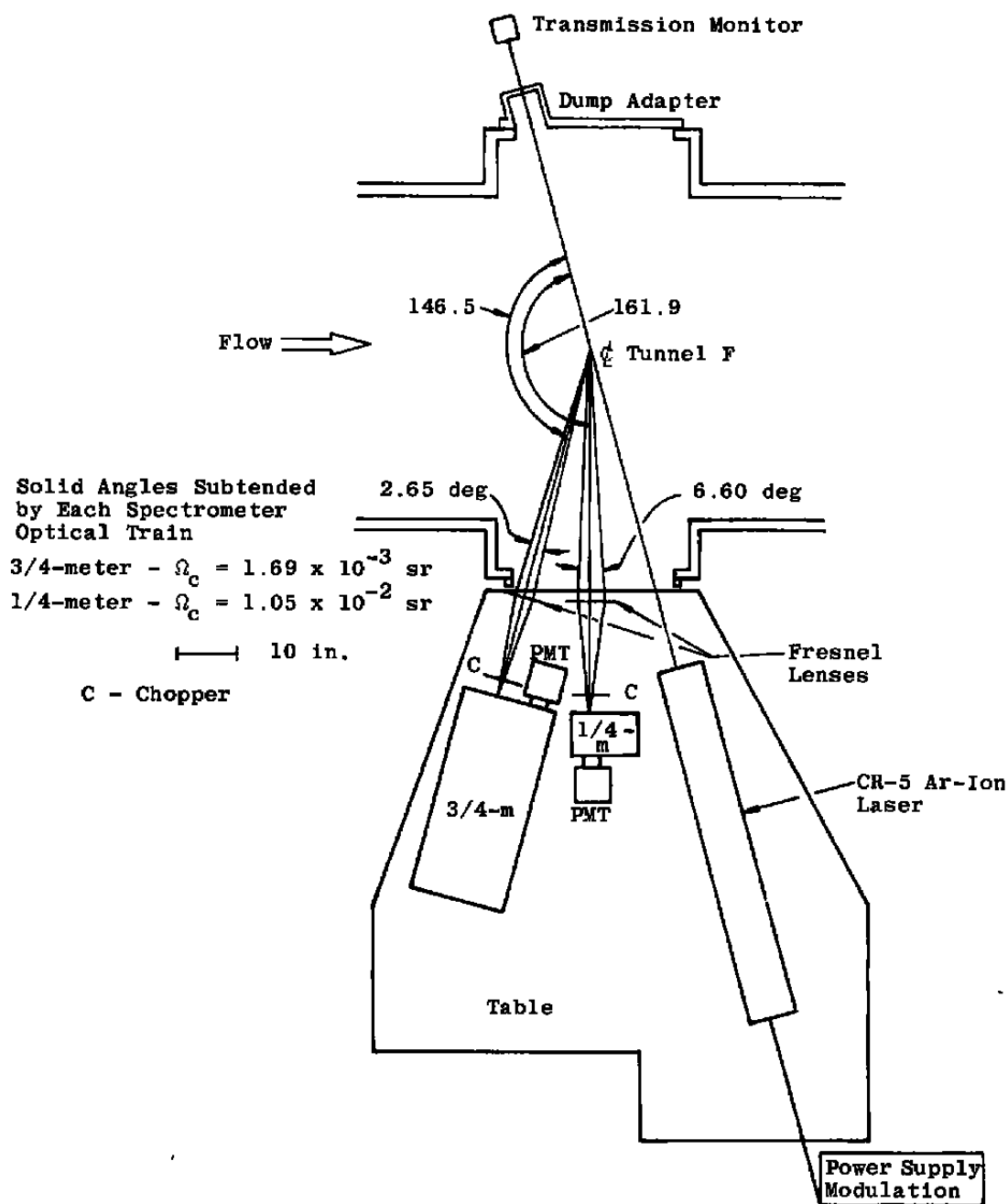
Figure 6. Schematic diagram of apparatus placement for the
Tunnel F sizing experiment.

$\overline{E}(\parallel)$

$\overline{E}(\parallel)$

$\overline{k}$

$\overline{E}(\perp)$

Detector

or

$\overline{E}(\perp)$

Chopper

Incident Field
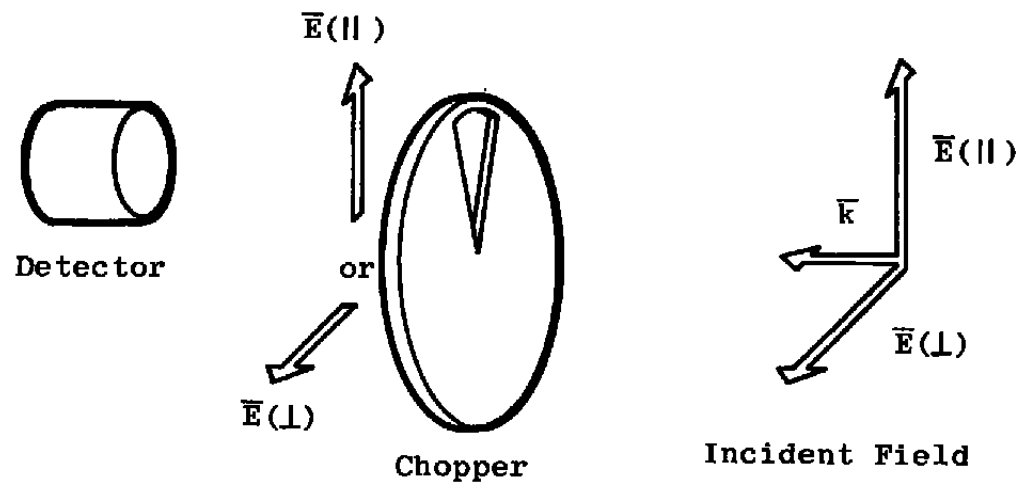
a. Schematic of components in optical path
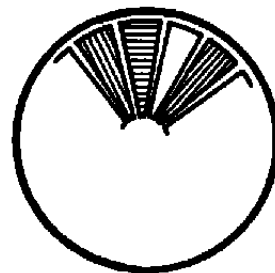
b. Partial view of chopper

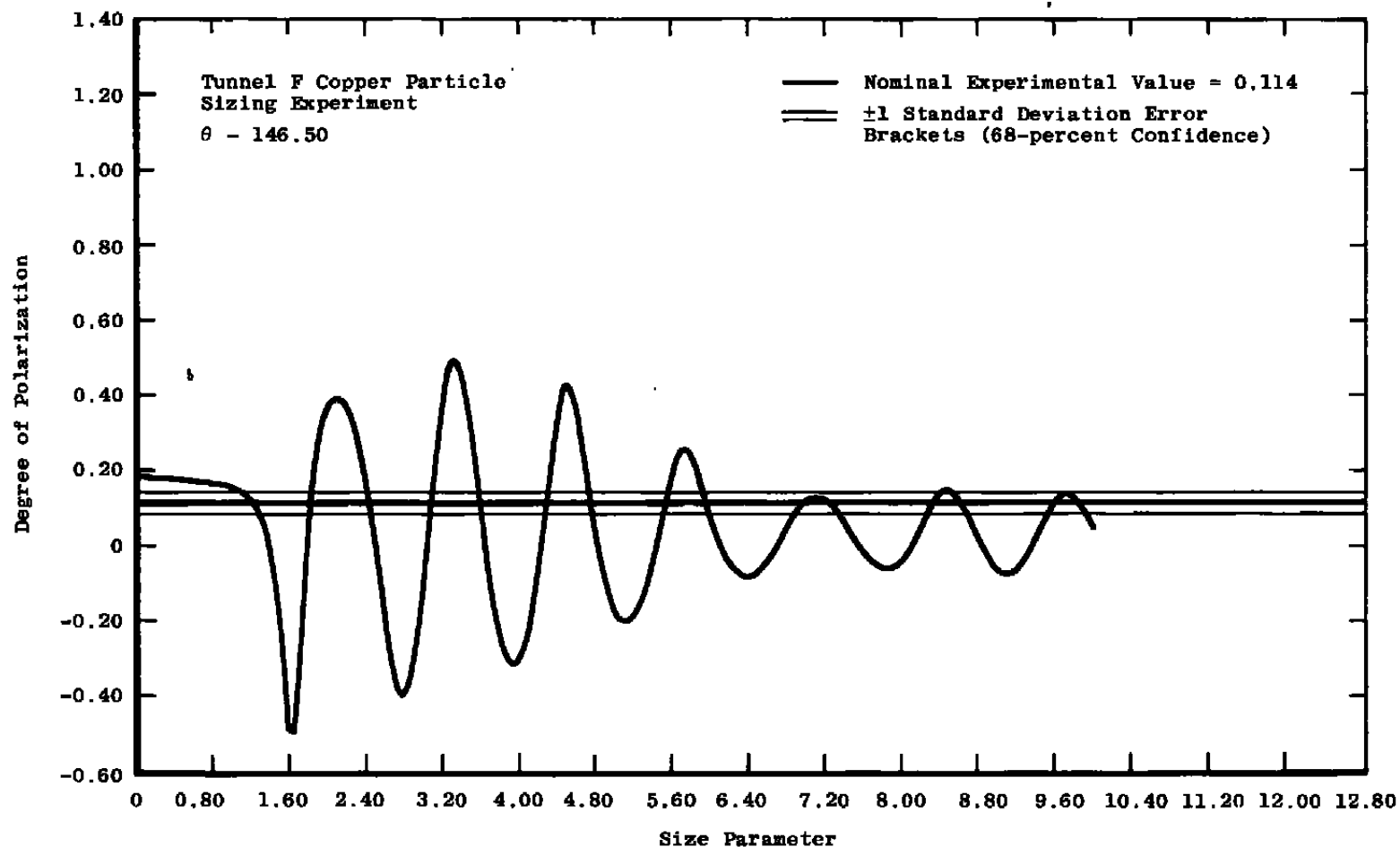Figure 7. Particle sizing detector channel configuration.

Figure 8. Calculated size dependence of degree of polarization with
superimposed range of measured values, θ = 146.5 deg.
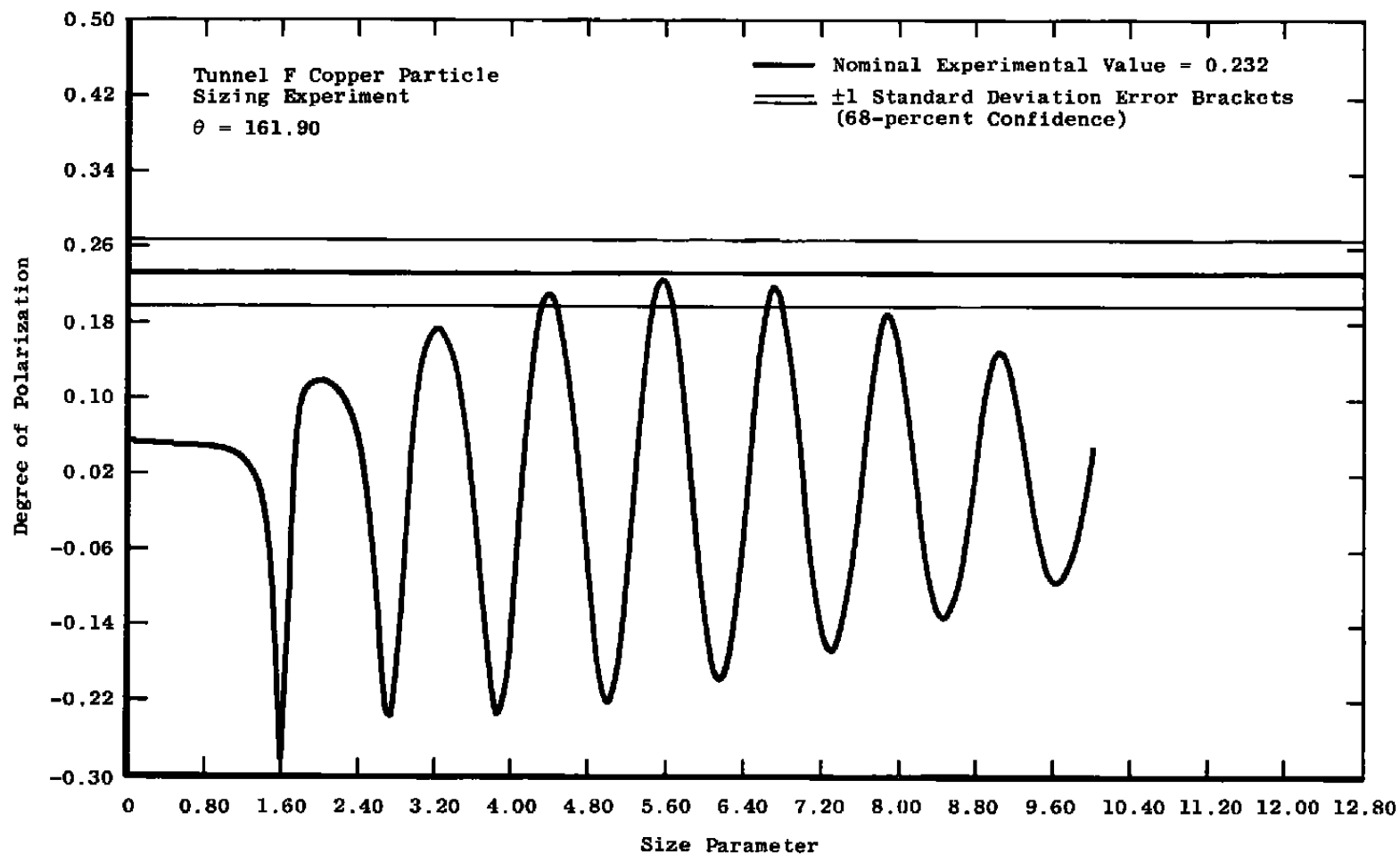
Figure 9. Calculated size dependence of degree of polarization with
superimposed range of measured values, θ = 161.9 deg.

Figure 10. Calculated size dependence of angular/extinction ratio with
superimposed range of measured values, θ = 146.5 deg,
perpendicular polarization.

Figure 11. Calculated size dependence of angular/extinction ratio with
superimposed range of measured values, θ = 146.5 deg,
parallel polarization.

Figure 12. Calculated size dependence of angular/extinction ratio with superimposed range of measured values, θ = 161.9 deg, perpendicular polarization.

Figure 13. Calculated size dependence of angular/extinction ratio with
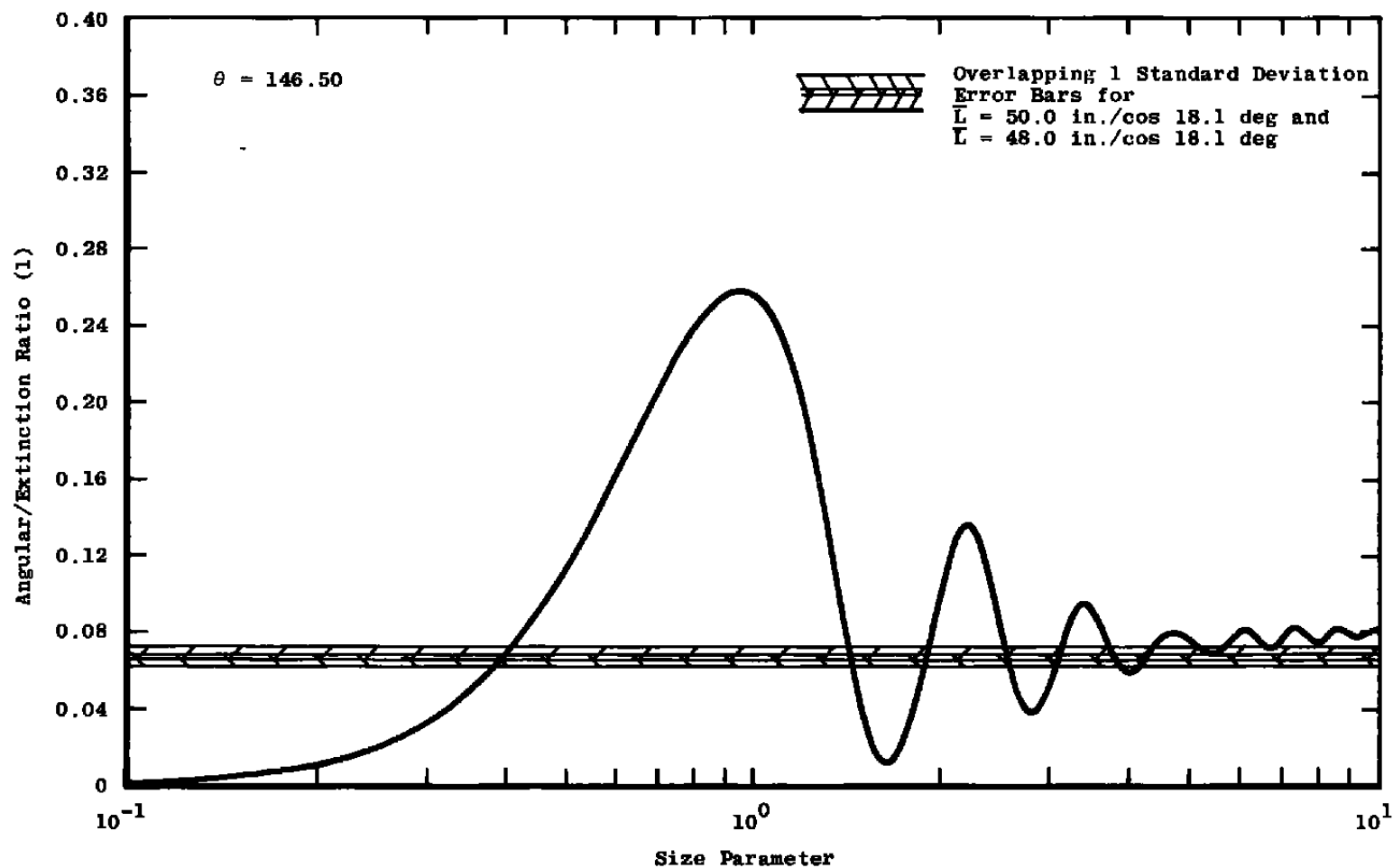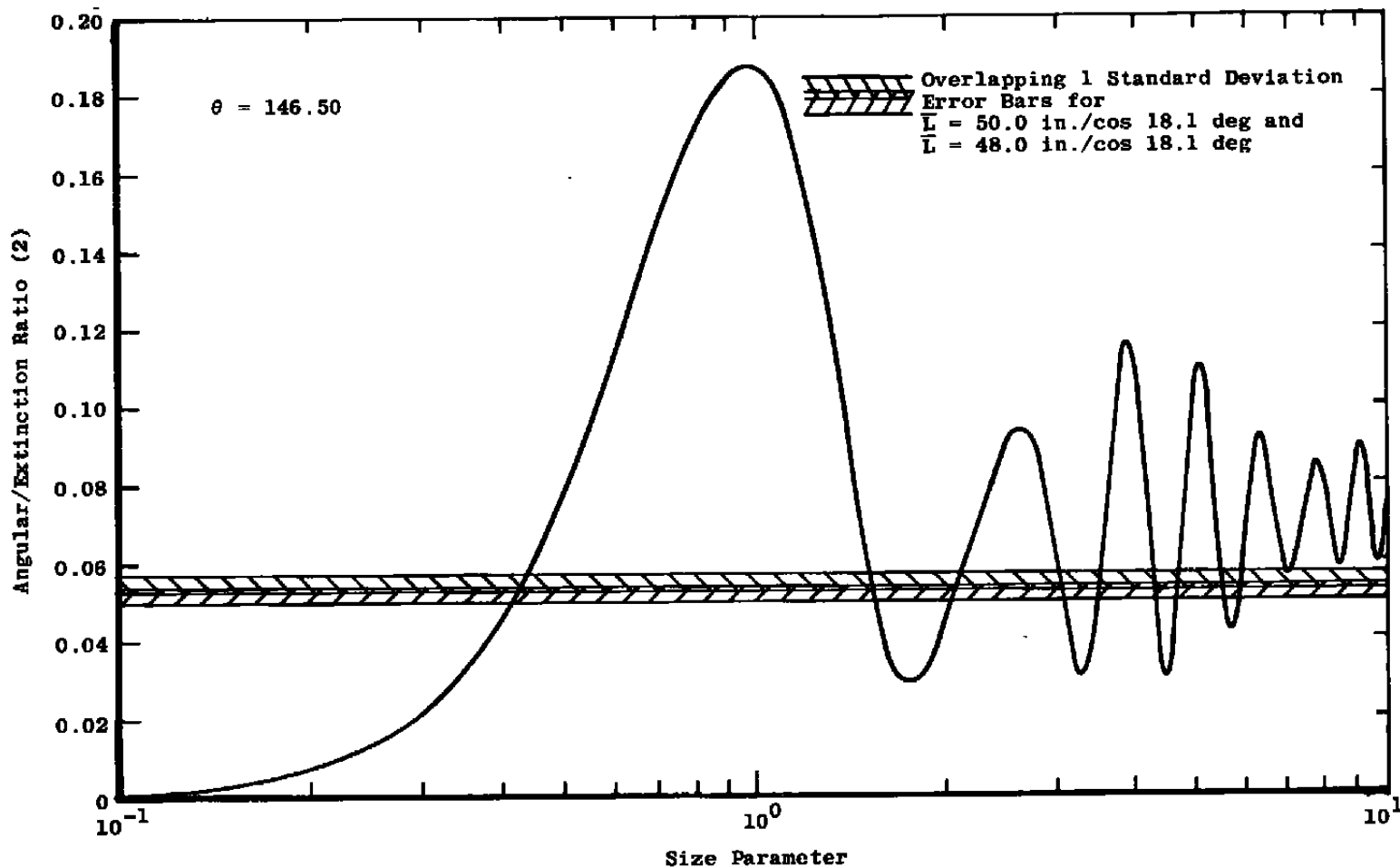superimposed range of measured values, $\theta = 161.9$ deg,
parallel polarization.

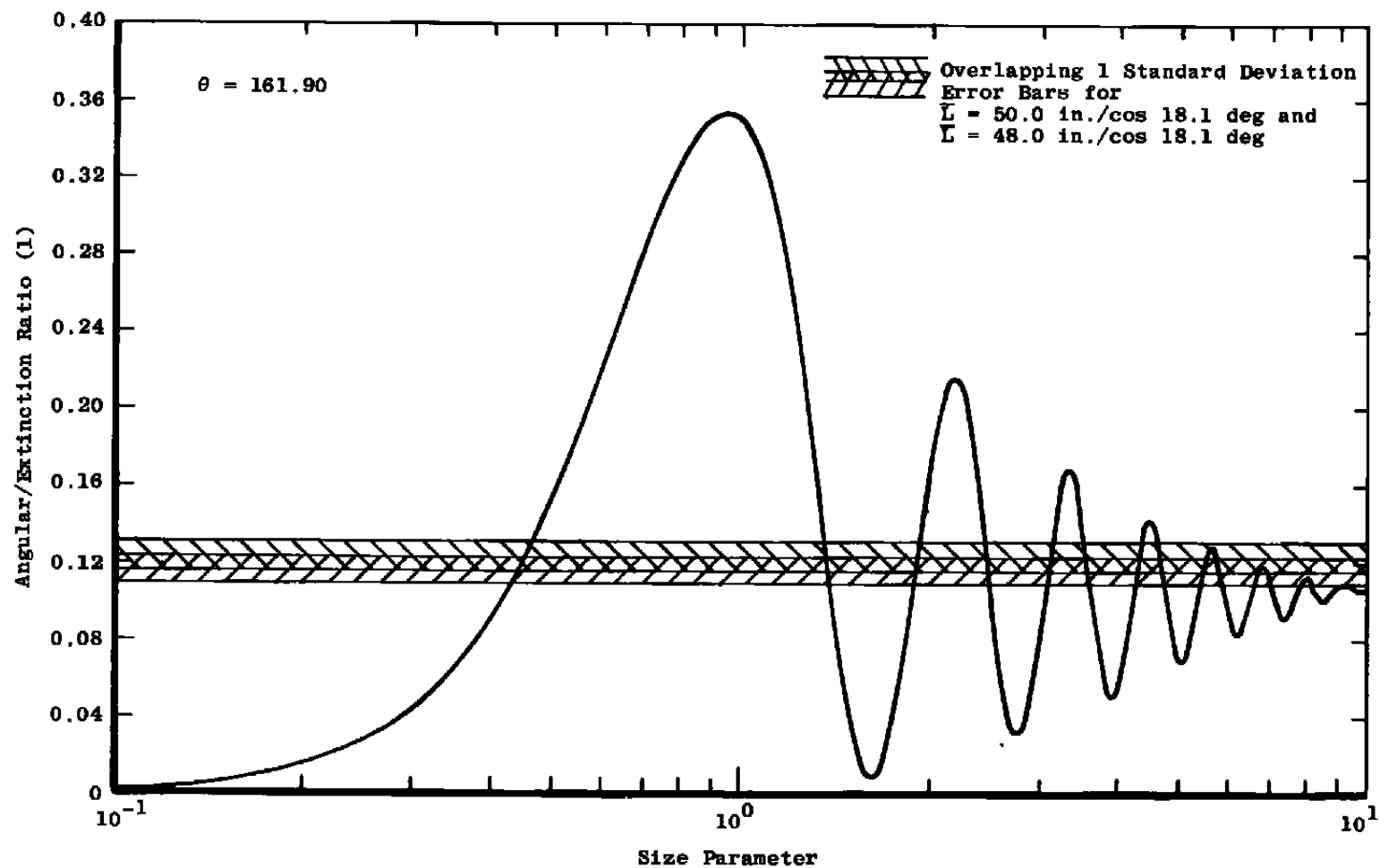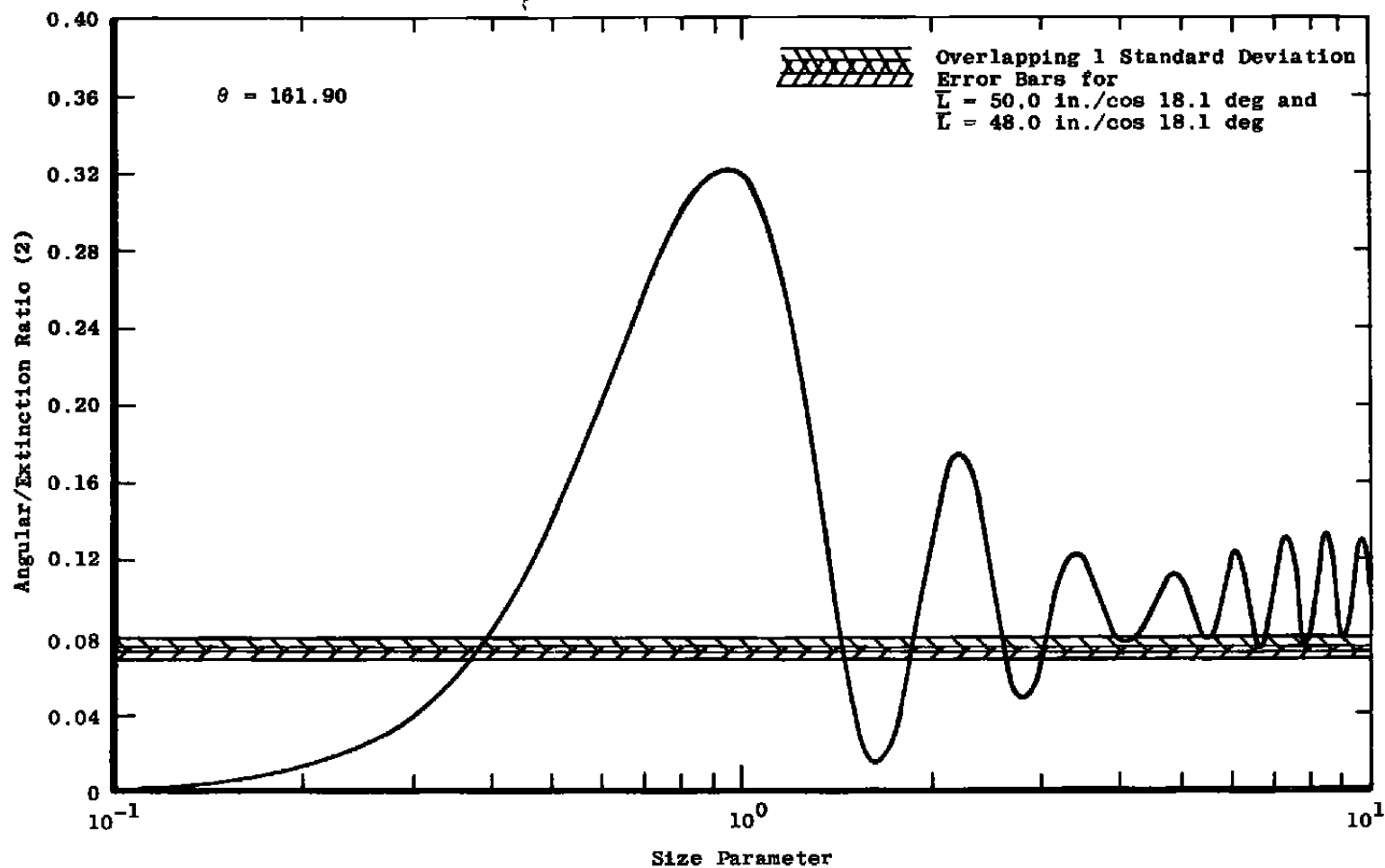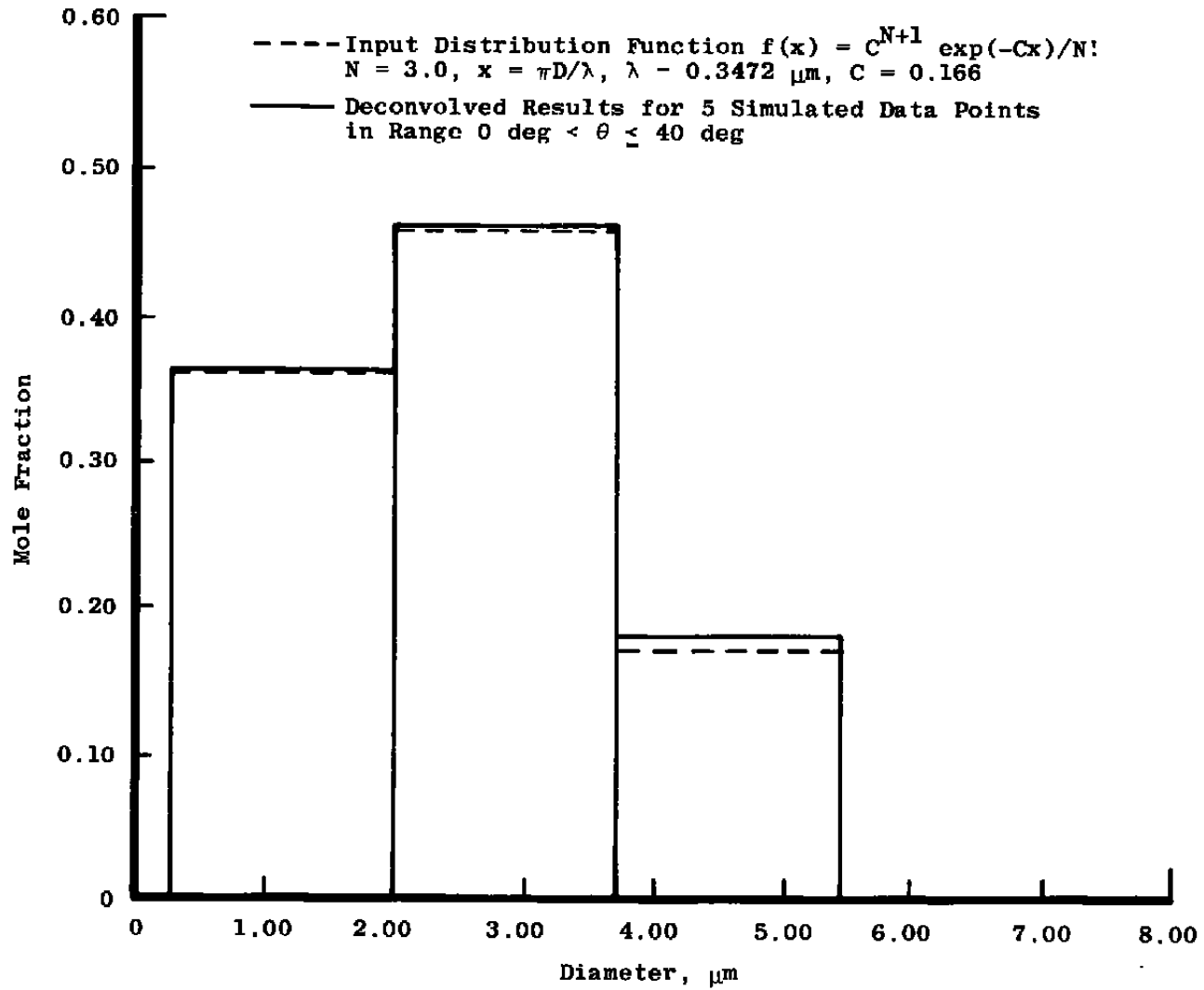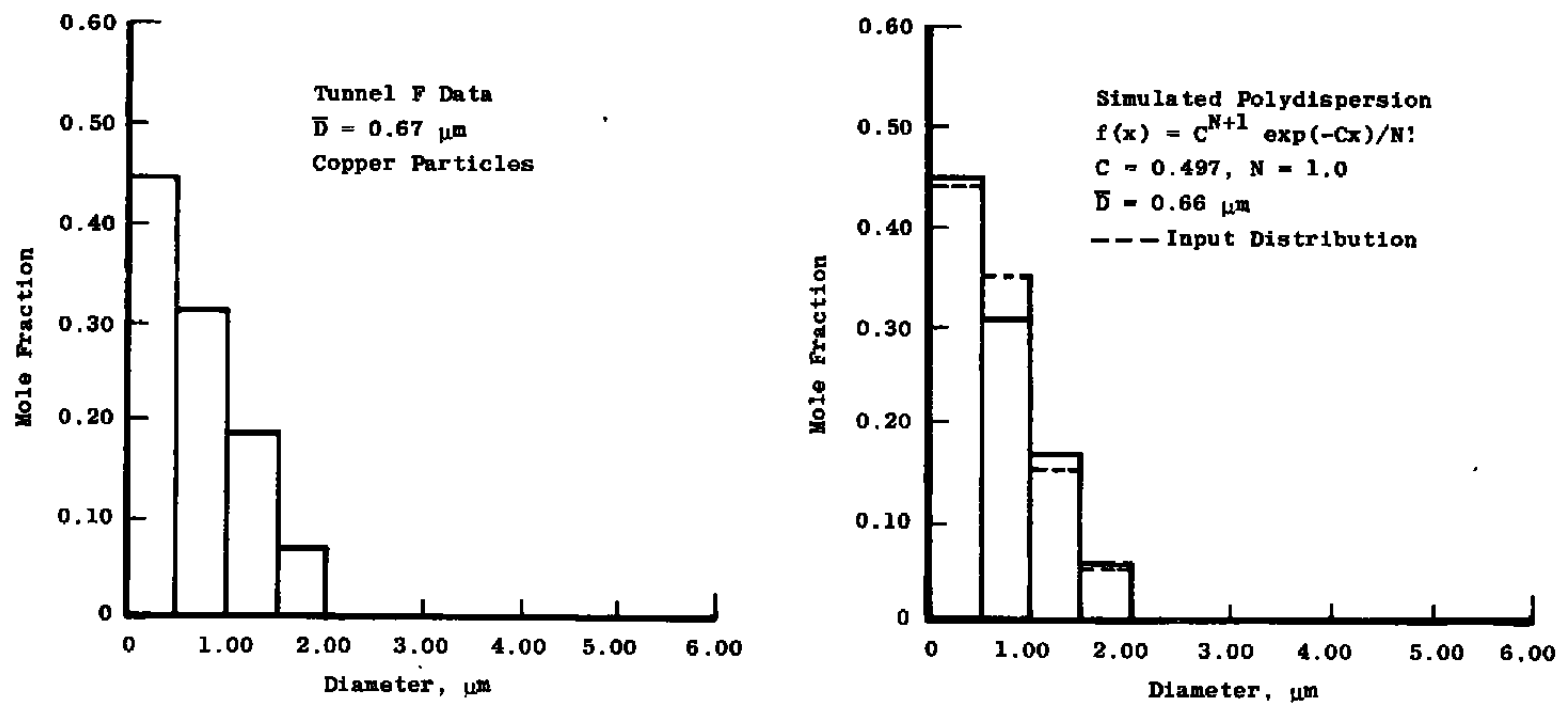Figure 14. Deconvolution of a simulated polydispersion.

Figure 15. Comparison of deconvolved Tunnel F sizing measurements with
simulated polydispersion deconvolution.

APPENDIX A
PHILLIPS-TWOMEY INVERSION PROCEDURE

In many areas of applied physics it is impossible to make direct measurements of some desired function of a quantity x, but, instead, one must infer the values of f(x) through complementary measurements of an associated function of a quantity y. The two parameters are often related by a Fredholm integral equation of the first kind.

$$g(y) = \int_0^\infty f(x) \, K(y, x) \, dx \qquad \text{(A-1)}$$

The relation between particle size distribution f(x) and scattered light intensity measurements distributed as functions of either wavelength or scattering angle is described by such an equation. When wavelength is the argument of inversion (y), the kernel takes an especially simple form $K(\lambda, D) => K(D/\lambda)$. In the limit of Rayleigh-Gans scattering, Eq. (A-1) has been inverted in closed form by use of Mellin transforms (Ref. A-1). When the more general case of Mie scattering is considered, such an approach must be abandoned because of the complex dependence of the Mie functions on size parameter $x = \pi D/\lambda$, although in principle the transforms could still be obtained numerically be exploiting the simplified form of the kernel. When the scattering angle is the argument, there is no symmetry in the dependence of the kernel on θ and on x, and the inversion must be accomplished by reduction to quadratures and the use of matrix inversion techniques.

The matrix analog of Eq. (A-1) is

$$g_i + \epsilon_i = K_{ij} F_j \qquad \text{(A-2)}$$

where

$$g_i = g(y_i)$$

$$K_{ij} = \int_{x_{j-1}}^{x_j} K(y_i, x) \, \frac{dx}{x_j - x_{j-1}}$$

$$F_j = \int_{x_{j-1}}^{x_j} F(x) \, dx$$

and ϵ_i represents the combination of experimental and computational errors (introduced by reduction to guadratures, replacement of the integral of a product by a product of

intervals, and truncation caused by repalcing ∞ with a finite x_{max}). Phillips (Ref. A-2) has observed that direct inversion of Eq. (A-2) neglecting such errors, leads to unphysical oscillations of the solution components F_j — even to negative values. He has introduced a variational technique to account for these errors, obtaining a least-squares fit to the true solution. Twomey has improved and generalized Phillips' procedure, obtaining solutions which include both the smoothest (in least-squares sense) solution consistent with a given level of the mean square error and the solution with the least deviation from a trial solution (Ref. A-3).

Dave has encoded the trial solution technique and obtained good results by deconvolving computer simulated polydispersions, but the deconvolution of actual scattering measurements has produced only fair results for the scattering from water droplets whose size distribution was independently determined using a Dessens trap (Ref. A-4). Dave's deconvolution was based on angular scattering data obtained and published by another investigator, and there is some doubt regarding the quality of the data. Chow and Tien (Ref. A-5) have tested the smoothing technique using computer simulated polydispersions and a large number of simulated angular intensity measurements. Their work showed that the distribution function can be accurately unfolded, even in the presence of simulated random errors.

Accounting for the error components ϵ_i and using the smoothest solution procedure we proceed as follows:

$$K_{ki}^{T} (g_i - \epsilon_i) = M_{kj}F_j, \quad M_{kj} = K_{ki}^{T}K_{ij} \tag{A-3}$$

Now, let

$$H(F_i) = F_{i+1} - 2F_i + F_{i-1}$$

and let

$$y = \gamma \Sigma_i (H(^2F_i) + \epsilon_i^2)$$

setting

$$\frac{\partial y}{\partial F_j} \equiv 0$$

gives

$$\Sigma_i \left[\gamma H(F_i) \, H'(F_i)\partial_{ij} - \epsilon_i \frac{\partial \epsilon_i}{\partial F_j} \right] = 0 \tag{A-4}$$

where γ is a lagrange multiplier.

Let

$$k_{ji} F_i = \Sigma_i \; H(F_i) \; H'(F_i) \; \delta_{ij}$$

Then it can be shown that

$$h_{ji} = \delta_{(j, i\pm 2)} - 4\delta_{(j, i\pm 1)} - 6\delta_{(j, i)} \quad \text{for } i, j > 2 \tag{A-5}$$

The requirement that the solution F_i can be continued to values of i less than 1.0 yields

$$h_{11} = 1, \; h_{12} = -2 = h_{21}, h_{22} = 5.$$

Other authors (notably Ref. A-5) have applied a similar continuation condition at the lower right corner of the smoothing matrix. Such a form does not appear in Twomey's original work, and it seems unjustifiable to us, since we wish to deconvolve the size distribution into a comparatively small number of bins.

Now that the form of the smoothing matrix has been determined, it is comparatively simple to incorporate it into the solution procedure. Note that

$$\frac{\partial g_i}{\partial F_j} = 0 = K_{ij} - \frac{\partial \epsilon_i}{\partial F_j} \tag{A-6}$$

Combining this result with Eqs. (A-4) and (A-3) and inserting the smoothing matrix yields

$$\left(M_{ki} + \gamma h_{ki} \right) F_i = D^T_{ki} g_i \equiv R_{ki} F_i \tag{A-7}$$

Therefore, the smoothest least squares solution, at a given level of mean square error is

$$F_i = K^{-1}_{jk} K^T_{ki} g_i \tag{A-8}$$

The associated error vector is obtained from Eq. (A-2).

$$\epsilon_i = K_{ij} F_j - g_i \quad \text{with RMS value} \quad \epsilon = \left(\sum_{i=1}^{N} \frac{1}{N} \epsilon_i^2 \right)^{1/2} \tag{A-9}$$

and the relative error is just

$$\left(\frac{\sum_{i=1}^{N} \epsilon_i^2}{\sum_{i=1}^{N} g_i^2} \right)^{1/2}$$

41

In practice, one increases γ (the smoothing parameter) until the computed relative error exceeds the estimated relative experimental error.

It is of some interest to consider the significance of these errors in order to understand the function of the smoothing process and why smoothing is necessary. Twomey has shown that unaccounted errors in the measurement set act to eliminate the information content of the highest frequency components of the Fourier transform of the kernel (Ref. A-6). In fact, the dimension of independence of the set of measurements being inverted must be reduced by one for each eigenvalue of the symmetrized kernel $K^T_{ik}K_{kj}$ which falls below a threshold value related to the mean square error (Ref. A-6). In effect, the kernel matrix is singular under these conditions. The smoothing procedure systematically suppresses the eigenvectors associated with the occurrence of each such near-singularity.

The structure of the symmetrized kernel and, hence, the solution vector F, changes drastically when the smoothing parameter has just the right value to suppress a given eigenvector and very slowly when the smoothing parameter has any other value. These critical values of the smoothing parameter occur near (but not necessarily equal to) the eigenvalues associated with the eigenvectors being suppressed. If the smoothing matrix were diagonal, the critical values of the smoothing parameter would equal the associated eigenvalues.

As observed in the text, Eq. (A-1) is suitable for inversion of absolute intensity measurements (as functions of scattering angle and/or wavelength), but it must be modified when intensity ratios are used as the argument of inversion. Consider a reference kernel $K(y_0,x)$ (which can be a linear combination of functions $\Sigma_i a_i K(y_i,x)$) with y_0 chosen so as to minimize the dependence of the kernel on x. Define a transformed kernel as

$$Q_{(y,x)} = \frac{K_{(y,x)}}{K_{(y_0,x)}}$$

Eq. (A-1) now becomes

$$g_{(y)} = \int_0^\infty Q(y,x)\,\overline{f}(x)\,dx \qquad\qquad (A-10)$$

where

$$\overline{f}(x) = f(x)\left[\frac{\int_0^\infty K_{(y_0,x)}\,dx}{\int_0^\infty K_{(y_0,x)}\,f(x)\,dx}\right]$$

Normalization is assured by setting

$$\bar{f}_{norm}(x) = \frac{\bar{f}(x)}{\int_0^\infty \bar{f}(x)\,dx}$$

It is apparent that the quantity in square brackets plays the role of a normalization constant and is $\simeq 1$ when $K_{(y_0,x)}$ varies more slowly with x than f(x).

REFERENCES

A-1. Shifrin, K. S. and Perelman, A. Ya. "The Determination of the Spectrum of Particles in a Dispersed System from Data on Its Transparency. Optics and Spectroscopy, Vol. 15, 1963, pp. 185-289.

A-2. Phillips, D. L. "A Technique for the Numerical Solution of Certain Integral Equations of the First Kind." Journal of the Association for Computing Machinery, Vol. 9, 1962, pp. 84-97.

A-3. Twomey, S. "On the Numerical Solution of Fredholm Integral Equations of the First Kind by the Inversion of the Linear System Produced by Quadrature." Journal of the Association for Computing Machinery, Vol. 10, 1963, pp. 97-101.

A-4. Dave, J. V. "Determination of Size Distribution of Spherical Polydispersions Using Scattered Radiation Data." Applied Optics, Vol. 10, 1971, pp. 2035-2044.

A-5. Chow, L. C. and Tien, C. L. "Inversion Technique for Determining the Droplet Size Distribution in Clouds: Numerical Examination." Applied Optics, Vol. 15, 1976, pp. 378-383.

A-6. Twomey, S. "The Application of Numerical Filtering to the Solution of Integral Equations Encountered in Indirect Sensing Measurements." Journal of the Franklin Institute, Vol. 279, 1965, pp. 95-109.

NOMENCLATURE

A   Scattering kernel integrals [defined by Eq. (19)]

B   Scattering kernel integrals [defined by Eq. (19)]

C   Parameter appearing in distribution function used in simulated deconvolution

D   Particle diameter, μm

D_{01} Mean diameter of first size bin

D_{12} Mean diameter of second size bin

d   Distance from scattering event to detector, cm

$E_{(\perp, \parallel)}$ Electric field vectors, perpendicular and parallel, respectively, to scattering plane (Fig. 1)

F_s Mole fraction of particles in "j^{th}" size bin

f(s)   Particle size distribution function

$\underline{g}$ 4-component vector [defined by Eq. (13)] used as input to deconvolution procedure

$\underline{h}$ Smoothing matrix defined in Appendix A

I   Intensity of light, w/cm^2

i   Mie intensity function [defined by Eq. (1)]

K   Kernel of integral equation

k   Wavenumber of incident light, cm^{-1}

L   Distance over which appreciable scattering and absorption occur

$\bar{L}$ Effective absorption length used in angular/extinction ratio sizing procedure

ℓ Length of scattering volume

$\underline{M}$ Symmetric scattering kernel matrix [defined by Eq. (A-3)]

N   Parameter appearing in distribution function used in simulated deconvolution

n   Particle number density

$\bar{n}$ Particle number density averaged over distance L

$P(\theta_s, x)$ Degree of polarization [(Eq. (6)]

$\underline{Q}$ Scattering kernel matrix [defined by Eqs. (14) and (15)]

Q_{ext} Extinction efficiency ratio

Q_T Scattering efficiency ratio

R   Reference denominator for scattering kernel matrix

$\underline{R}$ Smoothed symmetric scattering kernel matrix [defined by Eq. (A-7)]

R_e Particle Reynolds number relative to flow

$R_i(\theta_s)$ Angular/extinction ratio for "i^{th}" polarization state evaluated at scattering angle θ_s

$\tilde{V}$ Specific volume occupied by the average particle

X   Particle size parameter, dimensionless

$\hat{x}, \hat{y}, \hat{z}$ Coordinate axes shown in Fig. 1

y   Dummy variable appearing in integral inversion discussion in Appendix A

α Particle mass fraction

γ Smoothing parameter defined in Appendix A

ΔL Distance from nozzle throat to exit plane

Δm Total particle mass in flow after establishment of flow

$\Delta \theta$ Range of scattering angles subtended by detector

$\Delta \phi$ Range of azimuthal angles subtended by detector

$\underline{\epsilon}$ Error vector [defined by Eq. (A-2)]

η	Particle index of refraction relative to medium (in Section 5.0 only)
θ	Polar scattering angle (see Fig. 1), deg
λ	Wavelength of incident light in the scattering medium; also constant [Eqs. (9a) through (9c)] appearing in discussion of integral equations
ν	Gas viscosity
ξ	Dummy variable [Eq. (9a)] appearing in discussion of integral equations
$\approx$	Reference denominator [defined by Eqs. (11) and (12)] used in deconvolution procedure
ρ	Density
σ	Scattering cross section integrated over solid angle subtended by detector
$d\sigma/d\Omega$	Differential scattering cross section
σ_{ext}	Extinction cross section
σ_T	Scattering cross section integrated over 4π steradians and summed over polarization
τ	Characteristic times appearing in Section 5.0
Φ	Energy flux of light beam, w
ϕ	Azimuthal angles, deg (see Fig. 1)
$<>$	Denotes integration of enclosed quantity over the range of scattering angles subtended by the detector
$<n\sigma_{ext}\ell>$	Denotes average of $n\sigma_{ext}\ell$ over the length L

Subscripts

0	Incident
1	Denotes scattering state with electric field vector perpendicular to scattering plane
2	Denotes scattering state with electric field vector parallel to scattering plane

D   Denotes a property of particles of diameter D

F   Denotes a property of the flow

g   Denotes a property of the gas field

max   Denotes finite value of x at which size distribution function is truncated

p   Denotes a property of the particle field

s   Denotes measurements associated with the set of angles $\theta_s \phi_s$ on which a detector is centered

th   Denotes conditions evaluated at the nozzle throat

Tr   Denotes transmitted beam

v   Denotes conditions evaluated at the mean particle speed

∞ Denotes free-stream conditions

Superscripts

$-$ Denotes average over size distribution

$\wedge$ Denotes function appearing in discussion of integral equations [Eqs. (9a) through (9c)]

i,j   Matrix indices